

**Operator Expansions for Linear Waves: Parallel Implementation and  
Multilayer Inversion**

by

Zheng Fang

B.A. (University of Science and Technology of China) 2010

M.S. (University of Illinois at Chicago) 2012

Thesis submitted in partial fulfillment of the requirements  
for the degree of Doctor of Philosophy in Mathematics (Applied Mathematics)  
in the Graduate College of the  
University of Illinois at Chicago, 2015

Chicago, Illinois

Defense Committee:

David P. Nicholls, Chair and Advisor

Gerard Awanou

Jan Verschelde

Irina Nenciu

Thomas J. Royston, Bioengineering

Copyright by

Zheng Fang

2015

To my parents,

Fengying and Zhiman,

who gave me the most spiritual and economical support so far.

## ACKNOWLEDGMENTS

Firstly, I want to thank my Advisor Professor David P. Nicholls, as without his patient and insightful guidance, it would have been impossible for me to write this thesis, and my PhD life would never have been pleasant as it has been. His rigorous attitude in doing research and universal fraternity in treating students have an everlasting impression on me. Also, I want to thank all my committee members, Professor Jan Verschelde, Professor Gerard Awanou and Professor Irina Nenciu, and special thanks to Professor Thomas J. Royston, head of Bioengineering, who spent time reading my thesis and help improve my thesis.

I would also like to thank Professor Charles Knessl, who was my mentor and gave me so much careful guidance and encouragement during the first half of my PhD program. I also thank Professor Roman Shvydkoy, for his enthusiasm in teaching and research. And thank all the math teachers I've had class with during my PhD years.

Special thanks to my friends as well as USTC alumnus Yang Jiao, Hexi Ye and Xu Gao. You really make my life here rich and colorful. My girlfriend Ting Hu's comfort and company help me a lot during the writing of this thesis, I want to thank her a lot, and all the other friends I've made during my PhD years in the US as well.

## TABLE OF CONTENTS

<u>CHAPTER</u>	<u>PAGE</u>
<b>1 NAVIER’S EQUATION</b> . . . . .	1
1.1 Introduction . . . . .	1
1.1.1 Previous Work . . . . .	1
1.1.2 Boundary Perturbation Method . . . . .	2
1.1.3 Governing Equations . . . . .	4
1.1.4 Plane Harmonic Waves in Elastic Half-Space . . . . .	9
1.1.5 Outgoing Solutions . . . . .	13
1.2 The Displacement–Traction Operator . . . . .	14
1.2.1 Infinitesimal Deformations . . . . .	18
1.2.2 General Deformations . . . . .	21
1.3 Numerical Results . . . . .	25
1.3.1 Exact Solutions . . . . .	26
1.3.2 Complexity Analysis and Improvement . . . . .	27
1.3.3 Numerical Implementation . . . . .	30
1.3.4 Error Measurement . . . . .	31
1.3.5 Numerical Tests . . . . .	31
<b>2 INTERFACE RECOVERY</b> . . . . .	39
2.1 Introduction . . . . .	39
2.1.1 Previous Work . . . . .	39
2.2 Governing Equation . . . . .	40
2.3 Forward Problem . . . . .	44
2.3.1 Surface Data Expansions . . . . .	45
2.3.2 Operator Expansions of the Upward Propagator . . . . .	47
2.3.3 Operator Expansions of the Dirichlet-Neumann Operators . . . . .	51
2.3.4 Parallel Computing Results for Forward Solver using OpenMP . . . . .	59
2.3.5 Parallel Computing Results for Forward Solver using FFTW MPI . . . . .	61
2.4 Inverse Problem . . . . .	63
2.4.1 2D Linear Model . . . . .	64
2.4.2 Numerical Results for 2D Reconstruction . . . . .	66
<b>3 CONCLUSION</b> . . . . .	80
<b>APPENDIX</b> . . . . .	82
<b>APPENDIX</b> . . . . .	86

TABLE OF CONTENTS (Continued)

<u>CHAPTER</u>	<u>PAGE</u>
CITED LITERATURE . . . . .	87
VITA . . . . .	93

## LIST OF ABBREVIATIONS

BEM	Boundary Element Method
BIM	Boundary Integral Method
BPM	Boundary Perturbation Method
DNO	Dirichlet-Neumann Operator
DTO	Displacement-Traction Operator
FDM	Finite Difference Method
FE	Field Expansion
FEM	Finite Element Method
FFT	Fast Fourier Transform
FFTW	Fast Fourier Transform in the West
ODE	Ordinary Differential Equation
OE	Operator Expansion
OWC	Outgoing Wave Condition
PDE	Partial Differential Equation
SEM	Spectral Element Method

## SUMMARY

The propagation of linear elastic waves arise in a wide array of applications, for instance, in mechanical engineering, materials science, and the geosciences. Many configurations of interest can be effectively modeled as layers of isotropic, homogeneous materials separated by thin interfaces across which material properties vary rapidly. In the frequency domain one must solve a system of coupled elliptic partial differential equations, however, this can be greatly simplified in the instance of layered media by considering interface unknowns. To realize this, one must be able to produce normal stresses (tractions) at these interfaces and Dirichlet–Neumann Operators accomplish this. In this contribution we discuss a novel Boundary Perturbation approach to compute these operators in a rapid, high–order, and robust fashion.

In addition, we have also implemented a parallel version of the algorithm using OpenMP and FFTW-MPI, and investigated the inversion method for 2D interface reconstruction using this Operator Expansions approach.

## CHAPTER 1

### NAVIER'S EQUATION

“Part of this chapter were previously published as (1)”

#### 1.1 Introduction

The propagation of linear elastic waves in an inhomogeneous medium arises in a wide array of applications, for instance, in mechanical engineering (2), materials science (3), and the geosciences (4; 5). These disturbances are governed by the wave equation where the velocity of propagation depends upon the properties of the material in question (2; 6). In many applications, e.g. in the instance of plane-wave incident radiation, it is sufficient to compute the scattering at a single temporal frequency and thus, in light of the linear nature of the governing equations, one may adopt the frequency-domain approach as we do here resulting in a system of elliptic PDE to be solved.

##### 1.1.1 Previous Work

In many instances, the medium may be effectively modeled by two or more isotropic, homogeneous layers which are delineated by sharp interfaces across which the material properties vary rapidly. Furthermore, for many purposes these can be specified by graphs of (single-valued) functions which, additionally, are periodic. Many numerical algorithms have been devised for the simulation of this problem. “The Finite Difference (FDM) (7; 8), Finite Element (FEM) (9; 10), and Spectral Element (SEM) (11; 12) methods have been studied but suffer from the

fact that they discretize the full volume of the model which not only introduces a huge number of degrees of freedom, but also raises the difficult question of appropriately specifying a far-field boundary condition explicitly. Furthermore, the Finite Difference method, while simple to devise and implement is not well-suited to the complex geometries of general layered media”.

An attractive alternative are *surface* integral methods (13; 14) “(e.g. Boundary Integral Methods—BIM—or Boundary Element Methods—BEM) which only require a discretization of the layer *interfaces* (rather than the whole structure) and which, due to the choice of the Green’s function, enforce the far-field boundary condition exactly. These methods can deliver high-accuracy simulations with greatly reduced operation counts”, however, such formulations typically require not only the surface trace of the field (the displacement), but also the surface trace of the *normal derivative* of the field (the traction) in order to close the set of coupled boundary conditions. “Dirichlet–Neumann Operators” (DNOs), and their generalizations, perform the operation of mapping the Dirichlet trace to its unique Neumann trace and thus it is clear that these DNOs play a central role in surface formulations. Before proceeding, we point out that DNOs have been studied in many contexts and are alternatively known as “Dirichlet–to–Neumann Maps” (15; 16; 17) and “Steklov–Poincaré Operators” (18).

### 1.1.2 Boundary Perturbation Method

For many problems, the layer interface shapes are moderate deviations from an exactly solvable flat-layer (infinitesimal) configuration, in which case a perturbative approach is natural. In particular, there are many low-order theories for scattering problems going back to the classical work of Rayleigh (19) and Rice (20). In the general case we refer the interested reader

to (21; 22; 23; 24; 25; 26; 27; 28; 29; 30; 31; 32; 33; 34; 35), while specific to elasticity we suggest (36; 37; 38; 39; 40). Boundary Perturbation Methods (BPMs) are built upon this philosophy, and have been shown to be a rapid, accurate, and robust class of numerical procedures for this problem (see (41) for a complete discussion and list of references). BPMs built upon Operator Expansions (30; 42; 43; 44; 45; 46), Field Expansions (47; 48; 49; 50; 51), and Transformed Field Expansions (52; 53; 54; 55; 56) have proven to be highly successful within their domains of applicability (which is *not* restricted by the *size* of the perturbation (54)), and we follow the Operator Expansions (OE) philosophy in this thesis (though other BPM could be imagined based upon our work here).

While the developments in this contribution follow these to a certain degree, a fundamental complication of the equations of linear elastodynamics is their three-dimensional nature, not only of the independent variable, but also the unknown field. One well-known consequence of this property is that within a homogeneous medium there are *two* (body) propagation velocities, those of the primary (P-) and secondary (S-) waves. As we shall see, this plays a crucial role in our developments and distinguishes it *significantly* from previous work.

Our approach is a Fourier/Taylor method which expands the quasiperiodic scattered field in a (generalized) Fourier series in the spatial variable, and the field in powers of the interface deformation which we characterize by a single quantity,  $\varepsilon$ , which we view as an (not necessarily small (54)) amplitude/slope. In previous work it has been shown that the scattered fields depend *analytically* upon the parameter  $\varepsilon$  with the radius of convergence dependent on the smoothness of the interface perturbation (as rough as Lipschitz (57; 54; 58)). For smooth

deformations the field will be *jointly* analytic with respect to both spatial and perturbation variables which results in a numerical scheme which converges exponentially as the numerical parameters are refined.

### 1.1.3 Governing Equations

We refer the interested reader to the very clear description of Chapter 5 of Billingham & King (2) for the governing equations of the propagation of linear waves in a solid (see also the classical text by Achenbach (6)). To summarize these developments, we recall that for small (total) displacements

$$\underline{\mathbf{u}}^t = \underline{\mathbf{u}}^t(x, t), \quad x \in \mathbb{R}^3,$$

of an elastic body, the governing equations are Navier's equations

$$\rho \partial_t^2 \underline{\mathbf{u}}_i^t = \partial_j \sigma_{ij}(\underline{\mathbf{u}}^t),$$

where  $\rho$  is the undisturbed density of the elastic solid, considering the 3 dimensional nature of the displacement,

$$\underline{\mathbf{u}}^t = (\underline{\mathbf{u}}_1^t, \underline{\mathbf{u}}_2^t, \underline{\mathbf{u}}_3^t)$$

and  $\sigma_{ij}$  is the symmetric stress tensor expressing the constitutive relation

$$\sigma_{ij} = \lambda e_{kk} \delta_{ij} + 2\mu e_{ij}.$$

In these,  $\lambda$  and  $\mu$  are the Lamé constants, more specifically,

$$\lambda = \frac{\nu E}{(1 + \nu)(1 - 2\nu)}$$

$$\mu = \frac{E}{2(1 + \nu)}$$

where  $E$  is Young's modulus, and  $\nu$  is the Poisson ratio (2). The identity tensor is denoted by

$\delta_{ij}$ ,

$$\delta_{ij} = \begin{cases} 0, & i \neq j \\ 1, & i = j \end{cases}, \quad i, j = 1, 2, 3,$$

and  $e_{ij}$  is the strain tensor (6),

$$e_{ij} = (1/2) \{ \partial_j \underline{u}_i^t + \partial_i \underline{u}_j^t \}. \quad (1.1)$$

And  $e_{kk}$  is known as the dilatation, which reflects the change of volume of an elastic element,

is defined as

$$\Delta = e_{kk} = \partial_i \underline{u}_1^t + \partial_j \underline{u}_2^t + \partial_k \underline{u}_3^t \quad (1.2)$$

**Proposition 1.1.1.** *The vector form of Navier's equations is*

$$\rho \partial_t^2 \underline{u}^t = (\lambda + \mu) \nabla \operatorname{div} [\underline{u}^t] + \mu \Delta \underline{u}^t.$$

And if we seek time-harmonic solutions of form

$$\underline{\mathbf{u}}^t(\mathbf{x}, t) = e^{-i\omega t} \underline{\mathbf{u}}^t(\mathbf{x}),$$

Navier's equation becomes

$$\mu \Delta \underline{\mathbf{u}}^t + (\lambda + \mu) \nabla \operatorname{div} [\underline{\mathbf{u}}^t] + \omega^2 \rho \underline{\mathbf{u}}^t = 0. \quad (1.3)$$

*Proof.*

$$\begin{aligned} \rho \partial_t^2 \underline{\mathbf{u}}_i^t &= \partial_j \sigma_{ij}(\underline{\mathbf{u}}^t) = \partial_j (\lambda e_{kk} \delta_{ij} + 2\mu e_{ij}) \\ &= \lambda \delta_{ij} \partial_j e_{kk} + 2\mu \partial_j e_{ij} \\ &= \lambda \partial_i e_{kk} + 2\mu \partial_j \left( \frac{1}{2} (\partial_i \underline{\mathbf{u}}_j^t + \partial_j \underline{\mathbf{u}}_i^t) \right) \\ &= \lambda \partial_i (\partial_j \underline{\mathbf{u}}_j^t) + \mu (\partial_i \partial_j \underline{\mathbf{u}}_j^t + \partial_j \partial_j \underline{\mathbf{u}}_i^t) \\ &= (\lambda + \mu) \partial_i \partial_j \underline{\mathbf{u}}_j^t + \mu \partial_j \partial_j \underline{\mathbf{u}}_i^t \\ &= (\lambda + \mu) \nabla \operatorname{div} [\underline{\mathbf{u}}^t] + \mu \Delta \underline{\mathbf{u}}^t. \end{aligned}$$

Given that  $\underline{\mathbf{u}}^t$  is time harmonic, we have

$$\begin{aligned} \rho \partial_t^2 \underline{\mathbf{u}}_i^t &= \rho \partial_t^2 (e^{-i\omega t} \underline{\mathbf{u}}_i^t) \\ &= \rho (-i\omega)^2 e^{-i\omega t} \underline{\mathbf{u}}^t = -\rho \omega^2 e^{-i\omega t} \underline{\mathbf{u}}_i^t \end{aligned}$$

As well as

$$\begin{aligned} (\lambda + \mu)\nabla\operatorname{div} [\underline{\mathbf{u}}^t] + \mu\Delta\underline{\mathbf{u}}^t &= (\lambda + \mu)\nabla\operatorname{div} \left[ e^{-i\omega t}\mathbf{u}_i^t \right] + \mu\Delta e^{-i\omega t}\mathbf{u}_i^t \\ &= e^{-i\omega t}((\lambda + \mu)\nabla\operatorname{div} [\mathbf{u}_i^t] + \mu\Delta\mathbf{u}_i^t). \end{aligned}$$

From the proven vector form Naver's Equation we have

$$-\rho\omega^2 e^{-i\omega t}\mathbf{u}_i^t = e^{-i\omega t}((\lambda + \mu)\nabla\operatorname{div} [\mathbf{u}_i^t] + \mu\Delta\mathbf{u}_i^t)$$

canceling  $e^{-i\omega t}$  on both sides and moving all terms on to one side we get the (Equation 1.3)

□

**Proposition 1.1.2.** *The Naver's Equation (Equation 1.3) is equivalent to*

$$\Delta\phi^t + \left(\omega/c^{(1)}\right)^2 \phi^t = 0, \quad \Delta\psi^t + \left(\omega/c^{(2)}\right)^2 \psi^t = 0, \quad \operatorname{div} [\psi^t] = 0, \quad (1.4)$$

Given that

$$\mathbf{u}^t = \nabla\phi^t + \operatorname{curl}[\psi^t], \quad \operatorname{div} [\psi^t] = 0,$$

where  $c^{(1)} := \sqrt{(\lambda + 2\mu)/\rho}$  and  $c^{(2)} := \sqrt{\mu/\rho}$ .

*Proof.* Using the Helmholtz decomposition (2; 6), we know

$$\mathbf{u}^t = \nabla\phi^t + \operatorname{curl}[\psi^t], \quad \operatorname{div} [\psi^t] = 0,$$

for any sufficient smooth, rapidly decaying and periodic vector field  $\mathbf{u}^t$ . Plug it into (Equation 1.3), we get

$$\begin{aligned}
& \mu\Delta\mathbf{u}^t + (\lambda + \mu)\nabla\text{div}[\mathbf{u}^t] + \omega^2\rho\mathbf{u}^t \\
&= \mu\Delta[\nabla\phi^t + \text{curl}[\boldsymbol{\psi}^t]] + (\lambda + \mu)\nabla\text{div}[\nabla\phi^t + \text{curl}[\boldsymbol{\psi}^t]] + \omega^2\rho(\nabla\phi^t + \text{curl}[\boldsymbol{\psi}^t]) \\
&= \nabla[\mu\Delta\phi^t + \omega^2\rho\phi^t + (\lambda + \mu)\text{div}[\nabla\phi^t]] + \text{curl}[\mu\Delta\boldsymbol{\psi}^t + \omega^2\rho\boldsymbol{\psi}^t] + (\lambda + \mu)\nabla\text{div}[\text{curl}[\boldsymbol{\psi}^t]] \\
&= \nabla[(\lambda + 2\mu)\Delta\phi^t + \omega^2\rho\phi^t] + \text{curl}[\mu\Delta\boldsymbol{\psi}^t + \omega^2\rho\boldsymbol{\psi}^t] + 0 \\
&= 0
\end{aligned}$$

Note here we use the fact from vector calculus that for any vector field  $F$ , it holds that  $\text{div}[\text{curl}[F]] = 0$ . Now we choose a solution that satisfies

$$\begin{aligned}
(\lambda + 2\mu)\Delta\phi^t + \omega^2\rho\phi^t &= 0 & \mu\Delta\boldsymbol{\psi}^t + \omega^2\rho\boldsymbol{\psi}^t &= 0 \\
\Delta\phi^t + \frac{\omega^2\rho}{\lambda + 2\mu}\phi^t &= 0 & \Delta\boldsymbol{\psi}^t + \frac{\omega^2\rho}{\mu}\boldsymbol{\psi}^t &= 0 \\
\Delta\phi^t + \left(\omega/c^{(1)}\right)^2\phi^t &= 0 & \Delta\boldsymbol{\psi}^t + \left(\omega/c^{(2)}\right)^2\boldsymbol{\psi}^t &= 0
\end{aligned}$$

Which is equivalent to (Equation 1.4) based on the definition of  $c^{(1)}$  and  $c^{(2)}$ .

□

**Remark 1.1.3.** Note that  $c^{(1)}$  is larger than  $c^{(2)}$ , we also call  $c^{(1)}$  the primary wave (P-wave),  $c^{(2)}$  the secondary wave (S-wave) velocities,  $\phi^t$  is the scalar potential and  $\boldsymbol{\psi}^t$  is the vector potential respectively.

#### 1.1.4 Plane Harmonic Waves in Elastic Half-Space

The problem we focus on here is the reflection of an incident plane wave in an elastic half-space adjoining a medium which does not transmit mechanical waves. In particular, we focus upon incident plane-waves

$$\mathbf{u}^i = \mathbf{A}e^{i(\boldsymbol{\alpha}\cdot\tilde{\mathbf{x}}-\gamma x_3)}, \quad \mathbf{A} \in \mathbb{R}^3, \quad \boldsymbol{\alpha} = (\alpha_1, \alpha_2)^\top, \quad \tilde{\mathbf{x}} = (x_1, x_2)^\top, \quad (1.5)$$

impinging from above upon a periodic interface

$$x_3 = g(\tilde{\mathbf{x}}), \quad g(\tilde{\mathbf{x}} + \tilde{\mathbf{d}}) = g(\tilde{\mathbf{x}}), \quad \tilde{\mathbf{d}} = (\mathbf{d}_1, \mathbf{d}_2)^\top,$$

where the solid occupies the domain  $x_3 > g(\tilde{\mathbf{x}})$ .

**Proposition 1.1.4.** *The incident radiation (Equation 1.5) will satisfy (Equation 1.3) provided that either*

$$\gamma^2 = \left(\omega/c^{(1)}\right)^2 - |\boldsymbol{\alpha}|^2, \quad \text{and } \mathbf{A} \text{ parallel to } (\boldsymbol{\alpha}, -\gamma)^\top,$$

or

$$\gamma^2 = \left(\omega/c^{(2)}\right)^2 - |\boldsymbol{\alpha}|^2, \quad \text{and } \mathbf{A} \text{ orthogonal to } (\boldsymbol{\alpha}, -\gamma)^\top,$$

*Proof.* Case 1: Setting  $\mathbf{A} = \mathbf{a}(\alpha, -\gamma)^\top$  and  $\alpha^2 + \gamma^2 = (\omega/c^{(1)})^2 = \frac{\rho\omega^2}{\lambda+2\mu}$

$$\begin{aligned}
\Delta \mathbf{u}^t &= \Delta[\mathbf{a}(\alpha, -\gamma)e^{i(\alpha\tilde{x}-\gamma x_3)}] \\
&= \mathbf{A}((i\alpha)^2 + (-i\gamma)^2)e^{i(\alpha\tilde{x}-\gamma x_3)} \\
&= \mathbf{A}(-\alpha^2 - \gamma^2)e^{i(\alpha\tilde{x}-\gamma x_3)} \\
&= -\mathbf{A}\frac{\rho\omega^2}{\lambda+2\mu}e^{i(\alpha\tilde{x}-\gamma x_3)} \\
&= -\frac{\rho\omega^2}{\lambda+2\mu}\mathbf{u}^t
\end{aligned}$$

$$\begin{aligned}
\nabla \operatorname{div} [\mathbf{u}^t] &= \nabla \mathbf{A} \cdot (i\alpha, -i\gamma)e^{i(\alpha\tilde{x}-\gamma x_3)} \\
&= \nabla \mathbf{a}(i\alpha^2 + i\gamma^2)e^{i(\alpha\tilde{x}-\gamma x_3)} \\
&= i\mathbf{a}\frac{\rho\omega^2}{\lambda+2\mu}\Delta e^{i(\alpha\tilde{x}-\gamma x_3)} \\
&= i\mathbf{a}\frac{\rho\omega^2}{\lambda+2\mu} \cdot (i\alpha, -i\gamma)e^{i(\alpha\tilde{x}-\gamma x_3)} \\
&= -\frac{\rho\omega^2}{\lambda+2\mu}\mathbf{A} \cdot e^{i(\alpha\tilde{x}-\gamma x_3)} \\
&= -\frac{\rho\omega^2}{\lambda+2\mu}\mathbf{u}^t
\end{aligned}$$

thus we have

$$\begin{aligned}
\mu\Delta\mathbf{u}^t + (\lambda + \mu)\nabla\operatorname{div}[\mathbf{u}^t] + \omega^2\rho\mathbf{u}^t &= \mu\left(-\frac{\rho\omega^2}{\lambda + 2\mu}\mathbf{u}^t\right) + (\lambda + \mu)\left(-\frac{\rho\omega^2}{\lambda + 2\mu}\mathbf{u}^t\right) + \omega^2\rho\mathbf{u}^t \\
&= \left(\frac{-\mu}{\lambda + 2\mu} + \frac{-(\lambda + \mu)}{\lambda + 2\mu} + 1\right)\rho\omega^2\mathbf{u}^t \\
&= 0 \cdot \rho\omega^2\mathbf{u}^t = 0
\end{aligned}$$

Case 2:  $\mathbf{A} \cdot (\alpha, -\gamma) = 0$  and  $\alpha^2 + \gamma^2 = (\omega/c^{(2)})^2 = \frac{\rho\omega^2}{\mu}$ , then

$$\begin{aligned}
\Delta\mathbf{u}^t &= (-\alpha^2 - \gamma^2)\mathbf{u}^t \\
&= -\frac{\rho\omega^2}{\mu}\mathbf{u}^t \\
\nabla[\operatorname{div}[\mathbf{u}^t]] &= \nabla[\mathbf{A} \cdot (i\alpha, -i\gamma)e^{i(\alpha\bar{x} - \gamma x_3)}] \\
&= \nabla[0] = 0.
\end{aligned}$$

Thus we also have

$$\begin{aligned}
\mu\Delta\mathbf{u}^t + (\lambda + \mu)\nabla\operatorname{div}[\mathbf{u}^t] + \omega^2\rho\mathbf{u}^t &= \mu\left(-\frac{\rho\omega^2}{\mu}\mathbf{u}^t\right) + \omega^2\rho\mathbf{u}^t \\
&= -\omega^2\rho\mathbf{u}^t + \omega^2\rho\mathbf{u}^t \\
&= 0.
\end{aligned}$$

□

Such an incident plane-wave will generate scattered surface displacements,  $\mathbf{u}$ , satisfying the boundary condition

$$\mathbf{u}(\tilde{\mathbf{x}}, \mathbf{g}(\tilde{\mathbf{x}})) = \xi(\tilde{\mathbf{x}}) := -\mathbf{u}^i(\tilde{\mathbf{x}}, \mathbf{g}(\tilde{\mathbf{x}})).$$

Due to the linear character of the problem the scattered displacement also satisfies the Navier equation, cf. (Equation 1.3),

$$\mu\Delta\mathbf{u} + (\lambda + \mu)\nabla\text{div}[\mathbf{u}] + \omega^2\rho\mathbf{u} = 0, \quad (1.6)$$

and, upon appealing to the Helmholtz decomposition, the Helmholtz equations, c.f. (Equation 1.4),

$$\Delta\phi + \left(\omega/c^{(1)}\right)^2\phi = 0, \quad \Delta\psi + \left(\omega/c^{(2)}\right)^2\psi = 0, \quad \text{div}[\psi] = 0. \quad (1.7)$$

This problem is known to have a unique,  $\alpha$ -quasiperiodic,

$$\mathbf{u}(\tilde{\mathbf{x}} + \tilde{\mathbf{d}}, x_3) = e^{i\alpha\tilde{\mathbf{d}}}\mathbf{u}(\tilde{\mathbf{x}}, x_3),$$

solution which is outgoing (6).

### 1.1.5 Outgoing Solutions

To make the notion of outgoing solutions more precise, for  $x_3 > |g|_{L^\infty}$ , the exact solutions (given by the Rayleigh expansions) for the Helmholtz equations, (Equation 1.7), are

$$\phi(x) = \sum_{|p|=-\infty}^{\infty} \hat{\phi}(p) e^{i(\alpha(p)\cdot\tilde{x} + \gamma^{(1)}(p)x_3)}, \quad \psi(x) = \sum_{|p|=-\infty}^{\infty} \hat{\psi}(p) e^{i(\alpha(p)\cdot\tilde{x} + \gamma^{(2)}(p)x_3)}, \quad (1.8)$$

where  $\psi(x)$  must be divergence-free. In these formulas  $p = (p_1, p_2)^T \in \mathbb{N}^2$  (so that the summation notation above is shorthand for the double sum over all  $p \in \mathbb{N}^2$ ) and

$$\alpha(p) = \alpha + 2\pi \begin{pmatrix} p_1/d_1 \\ p_2/d_2 \end{pmatrix}$$

$$\gamma^{(j)}(p) = \begin{cases} \sqrt{(\omega/c^{(j)})^2 - |\alpha(p)|^2}, & |\alpha(p)|^2 < (\omega/c^{(j)})^2 \\ i \sqrt{|\alpha(p)|^2 - (\omega/c^{(j)})^2}, & |\alpha(p)|^2 > (\omega/c^{(j)})^2 \end{cases}, \quad j = 1, 2.$$

The outgoing wave condition is reflected in the choice of the positive signs before  $\gamma^{(j)}(p)$  in the expressions for  $\phi$  and  $\psi$  in (Equation 1.8).

With the definition of the wavevector

$$\kappa^{(j)}(p) := \begin{pmatrix} \alpha(p) \\ \gamma^{(j)}(p) \end{pmatrix},$$

we can write

$$\phi(x) = \sum_{|\mathbf{p}|=-\infty}^{\infty} \hat{\phi}(\mathbf{p}) e^{i\kappa^{(1)}(\mathbf{p}) \cdot x}, \quad \psi(x) = \sum_{|\mathbf{p}|=-\infty}^{\infty} \hat{\psi}(\mathbf{p}) e^{i\kappa^{(2)}(\mathbf{p}) \cdot x}, \quad i\kappa^{(2)}(\mathbf{p}) \cdot \hat{\psi}(\mathbf{p}) = 0.$$

We can now express the scattered elastic wave field as

$$\mathbf{u}(x) = \nabla\phi + \text{curl}[\psi] = \sum_{|\mathbf{p}|=-\infty}^{\infty} (i\kappa^{(1)}(\mathbf{p})) \hat{\phi}(\mathbf{p}) e^{i\kappa^{(1)}(\mathbf{p}) \cdot x} + \sum_{|\mathbf{p}|=-\infty}^{\infty} \left\{ (i\kappa^{(2)}(\mathbf{p})) \times \hat{\psi}(\mathbf{p}) \right\} e^{i\kappa^{(2)}(\mathbf{p}) \cdot x},$$

$$(i\kappa^{(2)}(\mathbf{p})) \cdot \hat{\psi}(\mathbf{p}) = 0. \quad (1.9)$$

**Remark 1.1.5.** In this expression the *scalar* coefficient  $\hat{\phi}(\mathbf{p})$  delivers the P-waves, while the *vector* quantity  $\{(i\kappa^{(2)}(\mathbf{p})) \times \hat{\psi}(\mathbf{p})\}$  gives the S-waves. Due to the orthogonality constraint

$$(i\kappa^{(2)}(\mathbf{p})) \cdot \hat{\psi}(\mathbf{p}) = 0,$$

the latter lies in a two-dimensional space which can be spanned by a vector in the vertical plane (the SV-waves) and one in the horizontal plane (the SH-waves). Therefore (Equation 1.9) captures all of the body waves which propagate in a homogeneous, isotropic solid.

## 1.2 The Displacement–Traction Operator

The fundamental object of our study is a generalized Dirichlet–Neumann Operator (DNO), namely the Displacement–Traction Operator (DTO), which we define here.

**Definition 1.2.1.** Consider the time-harmonic Navier's equations, (Equation 1.6),

$$\mu\Delta\mathbf{u} + (\lambda + \mu)\nabla\operatorname{div}[\mathbf{u}] + \omega^2\rho\mathbf{u} = \mathbf{0}, \quad x_3 > g(\tilde{\mathbf{x}}),$$

supplemented with displacement (Dirichlet) data

$$\mathbf{u}(\tilde{\mathbf{x}}, g(\tilde{\mathbf{x}})) = \xi(\tilde{\mathbf{x}}). \quad (1.10)$$

The unique,  $\alpha$ -quasiperiodic, outgoing solution delivers the surface traction (normal stress; Neumann) data

$$\nu_i(\tilde{\mathbf{x}}) = \sigma_{ij}(\mathbf{u})|_{x_3=g} N_j,$$

with normal

$$\mathbf{N} = (-\partial_1 g, -\partial_2 g, 1)^\top,$$

and the Displacement-Traction Operator (DTO),  $\mathbf{G}$ , is defined as the operation of computing  $\nu$  given  $\xi$ ,

$$\mathbf{G}(g) : \xi \rightarrow \nu.$$

**Remark 1.2.2.** In light of the relation

$$\sigma_{ij} = \lambda e_{kk}\delta_{ij} + 2\mu e_{ij},$$

we introduce the notation  $G = L + M$  where

$$L := \lambda e_{kk} \delta_{ij} N_j|_{x_3=g} = \lambda e_{kk} N_i|_{x_3=g}, \quad M := 2\mu e_{ij} N_j|_{x_3=g}. \quad (1.11)$$

**Proposition 1.2.3.** *The DTO depends linearly upon the Dirichlet data  $\xi$ , but the dependence on  $g$  is nonlinear.*

*Proof.* We assume  $w = u + v$ , where

$$w = (w_1, w_2, w_3) \quad u = (u_1, u_2, u_3) \quad v = (v_1, v_2, v_3)$$

By the definition of operators  $L$  and  $M$  (Equation 1.11), and definition of strain tensor (Equation 1.1) and dilatation (Equation 1.2), we have

$$\begin{aligned} L(w) &= \lambda(\partial_i w_i + \partial_j w_j + \partial_k w_k) N_i \\ &= \lambda(\partial_i (u_i + v_i) + \partial_j (u_j + v_j) + \partial_k (u_k + v_k)) N_i \\ &= \lambda(\partial_i u_i + \partial_j u_j + \partial_k u_k) N_i + \lambda(\partial_i v_i + \partial_j v_j + \partial_k v_k) N_i \\ &= L(u) + L(v). \end{aligned}$$

Similarily we have

$$\begin{aligned}
 M(w) &= 2\mu e_{ij} N_j = \mu(\partial_i w_j + \partial_j w_i) N_j \\
 &= \mu(\partial_i (u_j + v_j) + \partial_j (u_i + v_i)) N_j \\
 &= \mu(\partial_i u_j + \partial_j u_i) N_j + \mu(\partial_i v_j + \partial_j v_i) N_j \\
 &= M(u) + M(v).
 \end{aligned}$$

Also we have

$$L(0) = M(0) = 0$$

and for any constant  $m$ , we have

$$L(m \cdot w) = m \cdot L(w) \quad M(m \cdot w) = m \cdot M(w)$$

Thus both the operator  $L$  and operator  $M$  are linear with respect to Dirichlet data;

To understand that these operators depends non-linearly upon the shape of interface  $g$ , we can look at the operators in more details.

$$w = (w_i(x, g(x)), w_j(x, g(x)), w_k(x, g(x))) \quad x = (x_1, x_2)$$

$$\begin{aligned}
L(\mathbf{w}) &= \lambda(\partial_i w_i + \partial_j w_j + \partial_k w_k) N_i \\
&= \lambda (\partial_{x_1} w_i + \partial_{x_3} w_k \partial_1 g(x) + \partial_{x_2} w_i + \partial_{x_3} w_k \partial_2 g(x) + \partial_{x_3} w_k) \cdot (\partial_1 g(x), \partial_2 g(x), -1)^T
\end{aligned}$$

From the the above expression, we can see that the operator  $L$  contains terms like  $\partial_1 g \partial_1 g$ ,  $\partial_1 g \partial_2 g$  and  $\partial_2 g \partial_2 g$  which is non-linearly dependent upon  $g$   $\square$

Note that the dependence upon  $g$  is *analytic* and we use this fact to great effect to produce a robust high-order numerical algorithm.

### 1.2.1 Infinitesimal Deformations

Before coming to this, we begin with the (relatively) simple case of the DTO in the case of an infinitesimal (non-zero but vanishingly small) interface that we model by  $g \equiv 0$  with normal  $N_i = -\delta_{i3}$ . While this is not the focus of our study, it is the “base case” which allows us to address non-zero deformations.

The first step is to find the unique solution to Navier’s equation with displacement boundary condition, (Equation 1.10). From (Equation 1.9) we have

$$\begin{aligned}
\sum_{|p|=-\infty}^{\infty} \hat{\xi}(p) e^{i\alpha(p)\cdot\tilde{x}} &= \xi(\tilde{x}) = \mathbf{u}(\tilde{x}, 0) \\
&= \sum_{|p|=-\infty}^{\infty} \left[ (i\kappa^{(1)}(p)) \hat{\Phi}(p) + \left\{ (i\kappa^{(2)}(p)) \times \hat{\Psi}(p) \right\} \right] e^{i\alpha(p)\cdot\tilde{x}},
\end{aligned}$$

subject to  $(i\kappa^{(2)}(\mathbf{p})) \cdot \hat{\Psi}(\mathbf{p}) = 0$ . The solution is found by solving the *linear* system of equations

$$\begin{pmatrix} i\kappa^{(2)}(\mathbf{p}) \times & i\kappa^{(1)}(\mathbf{p}) \\ i\kappa^{(2)}(\mathbf{p})^\top & 0 \end{pmatrix} \begin{pmatrix} \hat{\Psi}(\mathbf{p}) \\ \hat{\Phi}(\mathbf{p}) \end{pmatrix} = \begin{pmatrix} \hat{\xi}(\mathbf{p}) \\ 0 \end{pmatrix},$$

which, for each  $\mathbf{p}$ , is four equations in four unknowns. We denote the solution map by

$$\hat{\Psi}(\mathbf{p}) = \mathcal{L}_\psi [\hat{\xi}(\mathbf{p})], \quad \hat{\Phi}(\mathbf{p}) = \mathcal{L}_\phi [\hat{\xi}(\mathbf{p})].$$

**Proposition 1.2.4.** *For any solution to the Navier's Equation of the form satisfying (Equation 1.9),*

*and  $\mathbf{g} = 0$  We have*

$$\mathbb{L}^{(0)}[\xi] = \sum_{|\mathbf{p}|=-\infty}^{\infty} \lambda \left| \kappa^{(1)}(\mathbf{p}) \right|^2 \mathcal{L}_\phi [\hat{\xi}(\mathbf{p})] e^{i\alpha(\mathbf{p}) \cdot \bar{\mathbf{x}}} \delta_{i3}. \quad (1.12)$$

*and*

$$\begin{aligned} \mathbb{M}^{(0)}[\xi] = & \mu \sum_{|\mathbf{p}|=-\infty}^{\infty} \left[ 2\kappa_j^{(1)}(\mathbf{p}) \kappa_i^{(1)}(\mathbf{p}) \mathcal{L}_\phi [\hat{\xi}(\mathbf{p})] \right. \\ & \left. + \kappa_j^{(2)}(\mathbf{p}) \left\{ \kappa^{(2)}(\mathbf{p}) \times \mathcal{L}_\psi [\hat{\xi}(\mathbf{p})] \right\}_i + \kappa_i^{(2)}(\mathbf{p}) \left\{ \kappa^{(2)}(\mathbf{p}) \times \mathcal{L}_\psi [\hat{\xi}(\mathbf{p})] \right\}_j \right] e^{i\alpha(\mathbf{p}) \cdot \bar{\mathbf{x}}} \delta_{j3}. \quad (1.13) \end{aligned}$$

*Proof.* If  $\mathbf{g} = 0$ , then

$$\mathbf{N} = (\partial_i \mathbf{g}, \partial_j \mathbf{g}, -1) = (0, 0, -1)$$

Regarding the operator  $L = L^{(0)}$ , from (Equation 1.9) we have

$$\begin{aligned}
e_{kk}(x) &= \partial_k u_k(x) \\
&= \sum_{|p|=-\infty}^{\infty} (i\kappa^{(1)}(p)) \cdot (i\kappa^{(1)}(p)) \hat{\phi}(p) e^{i\kappa^{(1)}(p) \cdot x} + \sum_{|p|=-\infty}^{\infty} \left\{ (i\kappa^{(2)}(p)) \times \hat{\psi}(p) \right\} \cdot (i\kappa^{(2)}(p)) e^{i\kappa^{(2)}(p) \cdot x} \\
&= \sum_{|p|=-\infty}^{\infty} (i\kappa^{(1)}(p))^2 \cdot \hat{\phi}(p) e^{i\kappa^{(1)}(p) \cdot x} + 0 \\
&= \sum_{|p|=-\infty}^{\infty} -\left| \kappa^{(1)}(p) \right|^2 \hat{\phi}(p) e^{i\kappa^{(1)}(p) \cdot x},
\end{aligned}$$

Note here we've used the fact that  $(i\kappa^{(2)}(p)) \times \hat{\psi}(p)$  is perpendicular to  $(i\kappa^{(2)}(p))$ . So

$$\begin{aligned}
L^{(0)}[\xi] &= \lambda e_{kk} N_i |_{x_3=0} \\
&= \lambda \sum_{|p|=-\infty}^{\infty} -\left| \kappa^{(1)}(p) \right|^2 \hat{\phi}(p) e^{i\kappa^{(1)}(p) \cdot x} (-\delta_{i3}) \\
&= \sum_{|p|=-\infty}^{\infty} \lambda \left| \kappa^{(1)}(p) \right|^2 \mathcal{L}_\phi [\hat{\xi}(p)] e^{i\alpha(p) \cdot \bar{x}} \delta_{i3}.
\end{aligned}$$

Similarly, for For  $M = M^{(0)}$  we compute

$$\begin{aligned}
\partial_j u_i(x) &= \sum_{|p|=-\infty}^{\infty} (i\kappa_j^{(1)}(p))(i\kappa_i^{(1)}(p)) \hat{\phi}(p) e^{i\kappa^{(1)}(p) \cdot x} \\
&\quad + \sum_{|p|=-\infty}^{\infty} (i\kappa_j^{(2)}(p)) \left\{ (i\kappa^{(2)}(p)) \times \hat{\psi}(p) \right\}_i e^{i\kappa^{(2)}(p) \cdot x},
\end{aligned}$$

again subject to  $(i\kappa^{(2)}(\mathbf{p})) \cdot \hat{\Psi}(\mathbf{p}) = 0$ . So

$$2e_{ij} = \partial_j u_i + \partial_i u_j = \sum_{|\mathbf{p}|=-\infty}^{\infty} 2(i\kappa_j^{(1)}(\mathbf{p}))(i\kappa_i^{(1)}(\mathbf{p}))\hat{\Phi}(\mathbf{p})e^{i\kappa^{(1)}(\mathbf{p})\cdot\mathbf{x}} \\ + \sum_{|\mathbf{p}|=-\infty}^{\infty} \left[ (i\kappa_j^{(2)}(\mathbf{p})) \left\{ (i\kappa^{(2)}(\mathbf{p})) \times \hat{\Psi}(\mathbf{p}) \right\}_i + (i\kappa_i^{(2)}(\mathbf{p})) \left\{ (i\kappa^{(2)}(\mathbf{p})) \times \hat{\Psi}(\mathbf{p}) \right\}_j \right] e^{i\kappa^{(2)}(\mathbf{p})\cdot\mathbf{x}},$$

and

$$\begin{aligned} M^{(0)}[\xi] &= 2\mu e_{ij} N_j|_{x_3=0} = -2\mu e_{ij} \delta_{j3} |_{x_3=0} \\ &= \mu \sum_{|\mathbf{p}|=-\infty}^{\infty} \left[ 2\kappa_j^{(1)}(\mathbf{p})\kappa_i^{(1)}(\mathbf{p})\hat{\Phi}(\mathbf{p}) \right. \\ &\quad \left. + \kappa_j^{(2)}(\mathbf{p}) \left\{ \kappa^{(2)}(\mathbf{p}) \times \hat{\Psi}(\mathbf{p}) \right\}_i + \kappa_i^{(2)}(\mathbf{p}) \left\{ \kappa^{(2)}(\mathbf{p}) \times \hat{\Psi}(\mathbf{p}) \right\}_j \right] e^{i\alpha(\mathbf{p})\cdot\tilde{\mathbf{x}}}\delta_{j3} \\ &= \mu \sum_{|\mathbf{p}|=-\infty}^{\infty} \left[ 2\kappa_j^{(1)}(\mathbf{p})\kappa_i^{(1)}(\mathbf{p})\mathcal{L}_\Phi [\hat{\xi}(\mathbf{p})] \right. \\ &\quad \left. + \kappa_j^{(2)}(\mathbf{p}) \left\{ \kappa^{(2)}(\mathbf{p}) \times \mathcal{L}_\Psi [\hat{\xi}(\mathbf{p})] \right\}_i + \kappa_i^{(2)}(\mathbf{p}) \left\{ \kappa^{(2)}(\mathbf{p}) \times \mathcal{L}_\Psi [\hat{\xi}(\mathbf{p})] \right\}_j \right] e^{i\alpha(\mathbf{p})\cdot\tilde{\mathbf{x}}}\delta_{j3}. \quad (1.14) \end{aligned}$$

□

### 1.2.2 General Deformations

We now move to the general setting of DTOs connected to non-trivial geometries with interface shaped by the graph of the function  $x_3 = g(\tilde{\mathbf{x}})$ . Of course this is generally quite a difficult problem and the key to our approach is to consider deformations of the form

$$g(\tilde{\mathbf{x}}) = \varepsilon f(\tilde{\mathbf{x}}),$$

which gives rise to expansions

$$\mathbf{u} = \mathbf{u}(x; \varepsilon) = \sum_{n=0}^{\infty} \mathbf{u}^{(n)}(x) \varepsilon^n, \quad \mathbf{L} = \mathbf{L}(\varepsilon) = \sum_{n=0}^{\infty} \mathbf{L}^{(n)} \varepsilon^n, \quad \mathbf{M} = \mathbf{M}(\varepsilon) = \sum_{n=0}^{\infty} \mathbf{M}^{(n)} \varepsilon^n,$$

that can be shown to be strongly convergent (52; 54; 58). We now outline the Method of Operator Expansions (OE) (30; 42; 59; 55) for simulating DTO in this setting of linear elastodynamics.

To begin our development consider the following  $\alpha$ -quasiperiodic, outgoing solution of the time-harmonic Navier's equation

$$\mathbf{u}(x; \mathbf{p}) = (i\kappa^{(1)}(\mathbf{p})) \hat{\Phi}(\mathbf{p}) e^{i\kappa^{(1)}(\mathbf{p}) \cdot x} + \left\{ (i\kappa^{(2)}(\mathbf{p})) \times \hat{\Psi}(\mathbf{p}) \right\} e^{i\kappa^{(2)}(\mathbf{p}) \cdot x}, \quad (1.15)$$

subject to  $(i\kappa^{(2)}(\mathbf{p})) \cdot \hat{\Psi}(\mathbf{p}) = 0$ . We note that, in terms of these, (Equation 1.9) can be written as

$$\mathbf{u}(x) = \sum_{|\mathbf{p}|=-\infty}^{\infty} \mathbf{u}(x; \mathbf{p}), \quad (i\kappa^{(2)}(\mathbf{p})) \cdot \hat{\Psi}(\mathbf{p}) = 0.$$

We now define the *surface* quantities

$$\mathbf{U}(\tilde{x}; \mathbf{g}, \mathbf{p}) := \mathbf{u}(\tilde{x}, \mathbf{g}(\tilde{x}); \mathbf{p}) \quad (1.16a)$$

$$\mathbf{K}(\tilde{x}; \mathbf{g}, \mathbf{p}) := \partial_{\mathbf{k}} \mathbf{u}_{\mathbf{k}}(\tilde{x}, \mathbf{g}(\tilde{x}); \mathbf{p}) \quad (1.16b)$$

$$\mathbf{E}_{ij}(\tilde{x}; \mathbf{g}, \mathbf{p}) := \{\partial_j \mathbf{u}_i(\tilde{x}, \mathbf{g}(\tilde{x}); \mathbf{p}) + \partial_i \mathbf{u}_j(\tilde{x}, \mathbf{g}(\tilde{x}); \mathbf{p})\}, \quad (1.16c)$$

and observe that, expressing  $g = \varepsilon f$ , these are analytic in  $\varepsilon$  so that

$$\{\mathbf{U}, \mathbf{K}, E_{ij}\}(\tilde{\mathbf{x}}; \varepsilon f, \mathbf{p}) = \sum_{n=0}^{\infty} \{\mathbf{U}^{(n)}(\tilde{\mathbf{x}}; \mathbf{p}), \mathbf{K}^{(n)}(\tilde{\mathbf{x}}; \mathbf{p}), E_{ij}^{(n)}(\tilde{\mathbf{x}}; \mathbf{p})\} \varepsilon^n.$$

We will derive forms for the  $\{\mathbf{U}^{(n)}, \mathbf{K}^{(n)}, E_{ij}^{(n)}\}$  in § A.

Turning to the operator  $L$ , from (Equation 1.11) we can write

$$L(\varepsilon f) [\mathbf{U}(\tilde{\mathbf{x}}; \varepsilon f, \mathbf{p})] = \lambda \mathbf{K}(\tilde{\mathbf{x}}; \varepsilon f, \mathbf{p}) \mathbf{N}_i|_{x_3 = \varepsilon f},$$

and expand

$$\begin{aligned} \left( \sum_{n=0}^{\infty} \varepsilon^n L^{(n)}(f) \right) \left[ \sum_{m=0}^{\infty} \mathbf{U}^{(m)}(\tilde{\mathbf{x}}; f, \mathbf{p}) \varepsilon^m \right] &= \lambda(\varepsilon \partial_1 f) \sum_{n=0}^{\infty} \mathbf{K}^{(n)}(\tilde{\mathbf{x}}; f, \mathbf{p}) \varepsilon^n \delta_{i1} \\ &+ \lambda(\varepsilon \partial_2 f) \sum_{n=0}^{\infty} \mathbf{K}^{(n)}(\tilde{\mathbf{x}}; f, \mathbf{p}) \varepsilon^n \delta_{i2} - \lambda \sum_{n=0}^{\infty} \mathbf{K}^{(n)}(\tilde{\mathbf{x}}; f, \mathbf{p}) \varepsilon^n \delta_{i3}. \end{aligned}$$

Equating at order zero we find

$$L^{(0)} [\mathbf{U}^{(0)}] = -\lambda \mathbf{K}^{(0)} \delta_{i3},$$

where

$$\begin{aligned} \mathbf{U}^{(0)} &= \mathbf{u}(\tilde{\mathbf{x}}, 0; \mathbf{p}) = (i\kappa^{(1)}(\mathbf{p})) \hat{\phi}(\mathbf{p}) e^{i\alpha(\mathbf{p}) \cdot \tilde{\mathbf{x}}} + \left\{ (i\kappa^{(2)}(\mathbf{p})) \times \hat{\psi}(\mathbf{p}) \right\} e^{i\alpha(\mathbf{p}) \cdot \tilde{\mathbf{x}}} = \hat{\xi}(\mathbf{p}) e^{i\alpha(\mathbf{p}) \cdot \tilde{\mathbf{x}}} \\ \mathbf{K}^{(0)} &= - \left| \kappa^{(1)}(\mathbf{p}) \right|^2 \hat{\phi}(\mathbf{p}) e^{i\alpha(\mathbf{p}) \cdot \tilde{\mathbf{x}}} = - \left| \kappa^{(1)}(\mathbf{p}) \right|^2 \mathcal{L}_{\phi} [\hat{\xi}(\mathbf{p})] e^{i\alpha(\mathbf{p}) \cdot \tilde{\mathbf{x}}}, \end{aligned}$$

so that we recover (Equation 1.12)

$$\mathbf{L}^{(0)} \left[ \hat{\xi}(\mathbf{p}) e^{i\alpha(\mathbf{p}) \cdot \tilde{\mathbf{x}}} \right] = \lambda \left| \kappa^{(1)}(\mathbf{p}) \right|^2 \mathcal{L}_\phi \left[ \hat{\xi}(\mathbf{p}) \right] e^{i\alpha(\mathbf{p}) \cdot \tilde{\mathbf{x}}} \delta_{i3}.$$

At order  $n > 0$  we find

$$\begin{aligned} \mathbf{L}^{(n)}(f) \left[ \hat{\xi}(\mathbf{p}) e^{i\alpha(\mathbf{p}) \cdot \tilde{\mathbf{x}}} \right] &= \mathbf{L}^{(n)}(f) \left[ \mathbf{U}^{(0)} \right] = -\lambda \mathbf{K}^{(n)}(f) \delta_{i3} \\ &+ \lambda (\partial_1 f) \mathbf{K}^{(n-1)}(f) \delta_{i1} + \lambda (\partial_2 f) \mathbf{K}^{(n-1)}(f) \delta_{i2} - \sum_{m=0}^{n-1} \mathbf{L}^{(m)}(f) \left[ \mathbf{U}^{(n-m)} \right]. \end{aligned} \quad (1.17)$$

In an exactly analogous fashion we can show that

$$\mathbf{M}(\varepsilon f) \left[ \mathbf{U}(\tilde{\mathbf{x}}; \varepsilon f, \mathbf{p}) \right] = 2\mu \mathbf{e}_{ij} \Big|_{x_3 = \varepsilon f} = \mu \cdot \mathbf{E}(\tilde{\mathbf{x}}; \varepsilon f, \mathbf{p}) \mathbf{N}_i \Big|_{x_3 = \varepsilon f},$$

After expanding the operators, we get

$$\begin{aligned} \left( \sum_{n=0}^{\infty} \varepsilon^n \mathbf{M}^{(n)}(f) \right) \left[ \sum_{m=0}^{\infty} \mathbf{U}^{(m)}(\tilde{\mathbf{x}}; f, \mathbf{p}) \varepsilon^m \right] &= \mu (\varepsilon \partial_1 f) \sum_{n=0}^{\infty} \mathbf{E}^{(n)}(\tilde{\mathbf{x}}; f, \mathbf{p}) \varepsilon^n \delta_{i1} \\ &+ \mu (\varepsilon \partial_2 f) \sum_{n=0}^{\infty} \mathbf{E}^{(n)}(\tilde{\mathbf{x}}; f, \mathbf{p}) \varepsilon^n \delta_{i2} - \lambda \sum_{n=0}^{\infty} \mathbf{E}^{(n)}(\tilde{\mathbf{x}}; f, \mathbf{p}) \varepsilon^n \delta_{i3}. \end{aligned}$$

Equating at order zero we find

$$\begin{aligned}
\mathbf{M}^{(0)} \left[ \hat{\boldsymbol{\xi}}(\mathbf{p}) e^{i\alpha(\mathbf{p}) \cdot \tilde{\mathbf{x}}} \right] &= \mathbf{M}^{(0)} \left[ \mathbf{U}^{(0)} \right] = \mu \mathbf{E}_{ij}^{(0)} \delta_{j3} \\
&= \mu \left[ 2\kappa_j^{(1)}(\mathbf{p}) \kappa_i^{(1)}(\mathbf{p}) \mathcal{L}_\phi \left[ \hat{\boldsymbol{\xi}}(\mathbf{p}) \right] \right. \\
&\quad \left. + \kappa_j^{(2)}(\mathbf{p}) \left\{ \kappa^{(2)}(\mathbf{p}) \times \mathcal{L}_\psi \left[ \hat{\boldsymbol{\xi}}(\mathbf{p}) \right] \right\}_i + \kappa_i^{(2)}(\mathbf{p}) \left\{ \kappa^{(2)}(\mathbf{p}) \times \mathcal{L}_\psi \left[ \hat{\boldsymbol{\xi}}(\mathbf{p}) \right] \right\}_j \right] \delta_{j3},
\end{aligned}$$

which recovers (Equation 1.13), and equating at order  $n$  it follows that

$$\begin{aligned}
\mathbf{M}^{(n)}(f) \left[ \mathbf{U}^{(0)} \right] &= -\mu \mathbf{E}_{i3}^{(n)}(f) + \mu(\partial_1 f) \mathbf{E}_{i1}^{(n-1)}(f) + \mu(\partial_2 f) \mathbf{E}_{i2}^{(n-1)}(f) \\
&\quad - \sum_{m=0}^{n-1} \mathbf{M}^{(m)}(f) \left[ \mathbf{U}^{(n-m)} \right]. \quad (1.18)
\end{aligned}$$

Of course the key to all of these developments is the derivation of useful forms for the  $\{\mathbf{U}^{(n)}, \mathbf{K}^{(n)}, \mathbf{E}_{ij}^{(n)}\}$

which we describe in Appendix § A.

### 1.3 Numerical Results

Now we show the numerical simulation results of our DTO solver in details, and compare the results with the *exact* solutions. From the  $L_\infty$  norm of the difference, we can see that our method achieves high efficiency and accuracy. Also from the configuration of the algorithm, we can also expect it's generalization in other applications.

### 1.3.1 Exact Solutions

Naturally, for a problem as complicated as what we consider here (that of non-trivial interfaces), there are no known exact solutions. Thus, to conduct a study on the convergence of our algorithm we will follow this rule: When implementing a solver for the homogeneous problem:

$$\begin{aligned} \mathcal{L}u &= 0 && \text{in } \Omega \\ \mathcal{B}u &= 0 && \text{at } \partial\Omega, \end{aligned}$$

it is usually not hard to develop a method for the related inhomogeneous problem:

$$\begin{aligned} \mathcal{L}u &= \mathcal{R} && \text{in } \Omega \\ \mathcal{B}u &= \mathcal{Q} && \text{at } \partial\Omega. \end{aligned}$$

For any function  $f$ , we can calculate

$$\mathcal{R}_f := \mathcal{L}f, \quad \mathcal{Q}_f := \mathcal{B}f,$$

and automatically knows a solution that solves the problem

$$\begin{aligned} \mathcal{L}u &= \mathcal{R}_f && \text{in } \Omega \\ \mathcal{B}u &= \mathcal{Q}_f && \text{at } \partial\Omega, \end{aligned}$$

e.g.  $\mathbf{u} = \mathbf{f}$ . Thus, we have a means to test the inhomogeneous solver in this (special) case. Here we specify  $\mathbf{f}$  such that  $\mathcal{R}_f \equiv 0$ . These exact solutions correspond to plane-wave *reflection* rather than *incidence*.

More specifically, we consider the functions, c.f. (Equation 1.15),

$$\mathbf{u}(\mathbf{x}; \mathbf{p}) = (i\kappa^{(1)}(\mathbf{p}))\hat{\Phi}(\mathbf{p})e^{i\kappa^{(1)}(\mathbf{p})\cdot\mathbf{x}} + \left\{ (i\kappa^{(2)}(\mathbf{p})) \times \hat{\Psi}(\mathbf{p}) \right\} e^{i\kappa^{(2)}(\mathbf{p})\cdot\mathbf{x}}, \quad (1.19)$$

which, for any choice of integer  $\mathbf{p}$ , real  $\hat{\Phi}(\mathbf{p})$ , and real three-vector  $\hat{\Psi}(\mathbf{p})$  such that  $i\kappa^{(2)}(\mathbf{p}) \cdot \hat{\Psi}(\mathbf{p}) = 0$ , satisfy Navier's equations (Equation 1.6) and is outgoing so that  $\mathcal{R}_f \equiv 0$ . Note that these functions satisfied different boundary conditions from incident plane wave. We can calculate the surface data from the way we construct  $\mathcal{Q}_f$

$$\begin{aligned} \xi(\tilde{\mathbf{x}}, \mathbf{g}(\tilde{\mathbf{x}}); \mathbf{p}) &= \mathbf{u}(\tilde{\mathbf{x}}, \mathbf{g}(\tilde{\mathbf{x}}); \mathbf{p}) \\ &= \left[ (i\kappa^{(1)}(\mathbf{p}))\hat{\Phi}(\mathbf{p})e^{i\gamma^{(1)}(\mathbf{p})\mathbf{g}(\tilde{\mathbf{x}})} + \left\{ (i\kappa^{(2)}(\mathbf{p})) \times \hat{\Psi}(\mathbf{p}) \right\} e^{i\gamma^{(2)}(\mathbf{p})\mathbf{g}(\tilde{\mathbf{x}})} \right] e^{i\alpha(\mathbf{p})\cdot\tilde{\mathbf{x}}}. \end{aligned}$$

Now we get a group of exact solutions to the inhomogeneous problem, which we can use to test our numerical algorithm for different types of interface  $\mathbf{g}(\tilde{\mathbf{x}})$ .

### 1.3.2 Complexity Analysis and Improvement

Before leaving our discussion of the numerical implementation, we address one (initially) subtle, but crucially important consideration which can be effectively demonstrated in the formula for  $L^{(n)}$  (Equation 1.17) and  $M^{(n)}$  (Equation 1.18). Careful inspection of these formulas

reveal its *recursive* nature: In order to compute  $L^{(n)}[\psi]$  one needs to evaluate  $L^{(n-1)}$  applied to the function  $U^{(1)}$  which, in turn requires the evaluation of  $L^{(n-2)}$  applied to  $U^{(1)}$ , etc.

**Proposition 1.3.1.** *The complexity for calculating all  $L^{(n)}$  and  $M^{(n)}$  are both  $\mathcal{O}(N_x^2 2^{n+1})$ .*

*Proof.* Firstly, from the formulas for  $\{U^{(n)}, K^{(n)}$  and  $E_{ij}^{(n)}\}$  in § A, we know that the computation cost for them is  $\mathcal{O}(1)$  for each of them.

If we use notation  $T(n)$  to stand for the time complexity for calculating  $L^{(n)}$ , then following the formula for  $L^{(n)}$ , we can write the following relationship:

$$T(n) = \mathcal{O}(1) + \sum_{m=0}^{n-1} T(m).$$

We know  $T(0) = N_x^2$  and if we set  $T(n) = \mathcal{O}(N_x^2 2^n)$ , we will see the equation holds. Thus the time complexity for calculating all  $L^{(n)}$  is

$$\sum_{m=0}^{n-1} T(m) = \sum_{m=0}^{n-1} N_x^2 2^m = \mathcal{O}(N_x^2 2^{n+1}).$$

Similarly the time complexity for calculating all  $M^{(n)}$  will be the same  $\mathcal{O}(N_x^2 2^{n+1})$ .

□

In previous work we have shown (60; 55) how adjointness properties of these operators can be used to reduce this to  $\mathcal{O}(N_x \log(N_x) n^2)$ , however, we have been unable (thusfar) to reproduce this success in this setting. However, there is an alternative which avoids the prohibitive factorial cost of a direct implementation of (Equation 1.17). For this we *store* at every perturbation

order the action of  $L^{(n)}$  as a matrix acting on the basis functions  $\exp(i\alpha(\mathbf{p}) \cdot \tilde{\mathbf{x}})$  evaluated at the equally spaced gridpoints  $\tilde{\mathbf{x}}_l$ . While this is far from optimal (at every perturbation order one must evaluate at every wavenumber  $\mathbf{p}$  which we represent, of order  $\mathcal{O}(N_x^2 n^2)$ ), it certainly makes our algorithm feasible.

**Proposition 1.3.2.** *Calculating the operators  $L^{(n)}$  and  $M^{(n)}$  acting on basis functions lowers the time complexity of computing DTOs to  $\mathcal{O}(N_x^2 n^2)$*

*Proof.* For each dimension of the 3 dimensional wave(displacement), we need  $N_x \cdot N_x$  many wave numbers to represent the solution. For each wave number in each dimension we need to calculate the DTO action on them.

If we use notation  $T(n)$  to stands for the time complexity for calculating  $L^{(n)}$  acting on one basis function in one dimension, then following the formula for  $L^{(n)}$ , we can write the following relationship:

$$T(n) = \mathcal{O}(1) + \sum_{m=0}^{(n-1)} \mathcal{O}(1) = \mathcal{O}(n)$$

Thus the time complexity for calculating all  $L^{(n)}$  is

$$\sum_{m=0} T(m) = \sum_{m=0} \mathcal{O}(m) = \mathcal{O}(n^2)$$

Thus the total complexity to calculate all  $L^{(n)}$  is

$$3 \cdot (N_x)^2 \mathcal{O}(n^2) = \mathcal{O}((N_x)^2 n^2)$$

Similarly the time complexity for calculating all  $M^{(n)}$  will be the same  $\mathcal{O}((N_x)^2 n^2)$ .  $\square$

### 1.3.3 Numerical Implementation

The description of our numerical scheme is not complicated which, in our view, is a distinct advantage of our method. Our Boundary Perturbation approach posits, for instance, an expansion of the traction in the form

$$\mathbf{v}(\tilde{\mathbf{x}}; \varepsilon) = \sum_{n=0}^{\infty} \mathbf{v}^{(n)}(\tilde{\mathbf{x}}) \varepsilon^n$$

and we seek as an approximation, the truncation of this Taylor series after  $N$  terms

$$\mathbf{v}^N(\tilde{\mathbf{x}}; \varepsilon) = \sum_{n=0}^N \mathbf{v}^{(n)}(\tilde{\mathbf{x}}) \varepsilon^n.$$

Without approximation we can recover the  $\mathbf{v}^{(n)}$  from the formulas (Equation 1.12) & (Equation 1.13) at order zero, and (Equation 1.17) & (Equation 1.18) for  $n > 0$ . Each function appears in these formulas will be represented by Fourier series with finite number of non-zero coefficients. Thus, each of the  $\mathbf{v}^{(n)}(\tilde{\mathbf{x}})$  can be spectrally approximated as

$$\mathbf{v}^{n, N_x}(\tilde{\mathbf{x}}) := \sum_{|\mathbf{p}|=-N_x/2}^{N_x/2-1} \hat{\mathbf{v}}^{(n)}(\mathbf{p}) e^{i\alpha(\mathbf{p}) \cdot \tilde{\mathbf{x}}}. \quad (1.20)$$

Products appearing in (Equation 1.12), (Equation 1.13), (Equation 1.17), and (Equation 1.18) are computed by fast convolutions via the Fast Fourier Transform (FFT) algorithm (61) and our final Fourier/Taylor approximation is

$$\mathbf{v}^{N, N_x}(\tilde{\mathbf{x}}; \varepsilon) := \sum_{n=0}^N \sum_{|p|=-N_x/2}^{N_x/2-1} \hat{\mathbf{v}}^{(n)}(p) e^{i\alpha(p) \cdot \tilde{\mathbf{x}}} \varepsilon^n. \quad (1.21)$$

### 1.3.4 Error Measurement

With these numerical approximations we can make error measurements versus the exact solutions (Equation 1.19). We choose to measure the defect in the traction which is quite difficult, because this data is on the perturbed interface  $\mathbf{g}(\mathbf{x})$ . we measure the relative supremum norm of the results in § 1.3.5,

$$\text{Error}_{\text{rel}}(N, N_x) = \frac{|\mathbf{v} - \mathbf{v}^{N, N_x}|_{L^\infty}}{|\mathbf{v}|_{L^\infty}}. \quad (1.22)$$

### 1.3.5 Numerical Tests

We now consider a  $(2\pi) \times (2\pi)$  periodic interface bounding a three-dimensional solid. We follow the lead of (53; 62) and select the following interface shapes: The cosine

$$f_s(\mathbf{x}_1, \mathbf{x}_2) = \cos(\mathbf{x}_1 + \mathbf{x}_2), \quad (1.23a)$$

the analytic profile,

$$f_a(\mathbf{x}_1, \mathbf{x}_2) = W(\mathbf{x}_1)W(\mathbf{x}_2), \quad (1.23b)$$

where

$$W(z) = \frac{B^2 \cos(z) - B}{B^2 + 1 - 2B \cos(z)}, \quad B = (2\rho)^{-1/(R-1)}, \quad \rho = 10^{-16}, \quad R = 10,$$

the “rough” ( $C^2$  but not  $C^3$ ) profile

$$f_r(x_1, x_2) = \left(\frac{2}{9} \times 10^{-3}\right) \left\{ x_1^2(2\pi - x_1)^2 x_2^2(2\pi - x_2)^2 - \frac{64\pi^8}{225} \right\}, \quad (1.23c)$$

and the Lipschitz boundary

$$f_L(x_1, x_2) = \frac{1}{3} + \begin{cases} -1 + (2/\pi)x_1, & x_1 \leq x_2 \leq 2\pi - x_1 \\ 3 - (2/\pi)x_2, & x_2 > x_1, x_2 > 2\pi - x_1 \\ 3 - (2/\pi)x_1, & 2\pi - x_1 < x_2 < x_1 \\ -1 + (2/\pi)x_2, & x_2 < x_1, x_2 < 2\pi - x_1 \end{cases}. \quad (1.23d)$$

These four profiles share some common properties: (1) they have zero mean; (2) the approximate amplitude of them is 2; (3) the maximum slop is near 1. To clarify the choice of analytic profile  $f_a$  we point out (62) that the Fourier coefficients of  $W$  are

$$\hat{W}_p = \begin{cases} \frac{1}{2}(2\rho)^{(|p|-1)/(R-1)} & p \neq 0 \\ 0 & p = 0 \end{cases}$$

so that the profile has mean zero,  $\hat{W}_1 = \hat{W}_{-1} = 1/2$  like the cosine, the coefficients decay exponentially fast (giving analyticity of the profile), and the  $R$ -th coefficient has value  $\rho$ .

In Figures Figure 1 through Figure 4, we display results of our numerical simulations for the cosine profile(Equation 1.23a), analytic profile(Equation 1.23b),  $C^2$  profile(Equation 1.23c), and Lipschitz profile(Equation 1.23d) respectively, for values of  $\varepsilon = 10^{-3}, 3 \times 10^{-3}, 10^{-2}, 3 \times 10^{-2}$ . For physical parameters we picked values meant to be representative of steel (2)

$$\rho = 7800, \quad \lambda = 8.6 \times 10^{10}, \quad \mu = 7.9 \times 10^{10},$$

so that  $c^{(1)} \approx 5600$  and  $c^{(2)} \approx 3180$ , and the academic value  $\omega = 8000$  under normal illumination so that

$$\left| \kappa^{(1)} \right| = \omega/c^{(1)} \approx 1.429, \quad \left| \kappa^{(2)} \right| = \omega/c^{(2)} \approx 2.516.$$

For all four simulations we have chosen numerical parameters  $N_{x_1} = N_{x_2} = 8$  and perturbation orders  $N = 0, \dots, 10$ . In all four cases we see the rapid and stable convergence which our algorithm delivers in agreement with the spectral properties our Fourier/Taylor approach should enjoy.

TABLE I

COMMON PARAMETERS USED FOR NUMERICAL SIMULATIONS

Parameter	value	meaning
N	10	perturbation orders
$d_1$	$2\pi$	period in x direction
$d_2$	$2\pi$	period in y direction
$N_{x_1}$	16	number of grid points in x direction
$N_{x_2}$	16	number of grid points in y direction
$c^{(1)}$	5600	the speed of P-wave
$c^{(2)}$	3180	the speed of S-wave
$\omega$	8000	angular frequency
$\rho$	7800	the density of the material
$\lambda$	$8.6 \times 10^{10}$	Lame's first parameter
$\mu$	$7.9 \times 10^{10}$	Lame's second parameter
$ \kappa^{(1)} $	1.429	magnitude of wavenumber of P-wave
$ \kappa^{(2)} $	2.516	magnitude of wavenumber of S-wave

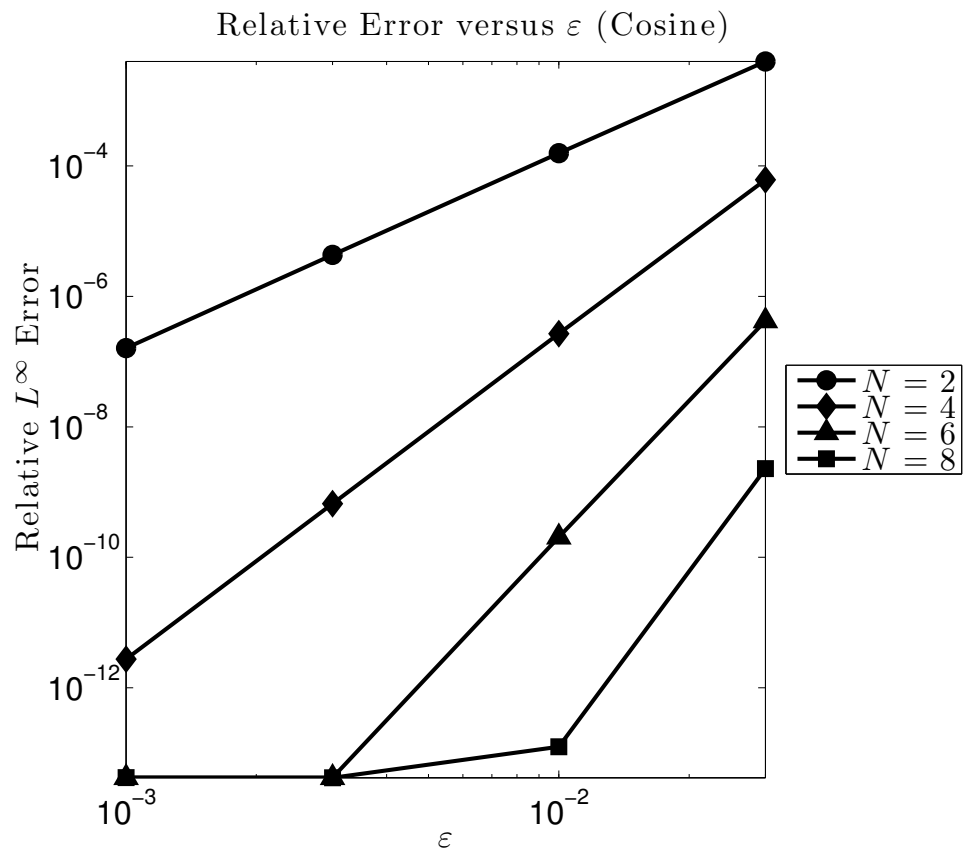


Figure 1. Plot of relative  $L^\infty$  error versus perturbation order  $N$  for the cosine profile, (Equation 1.23a) ( $\varepsilon = 10^{-3}, 3 \times 10^{-3}, 10^{-2}, 3 \times 10^{-2}$ ).

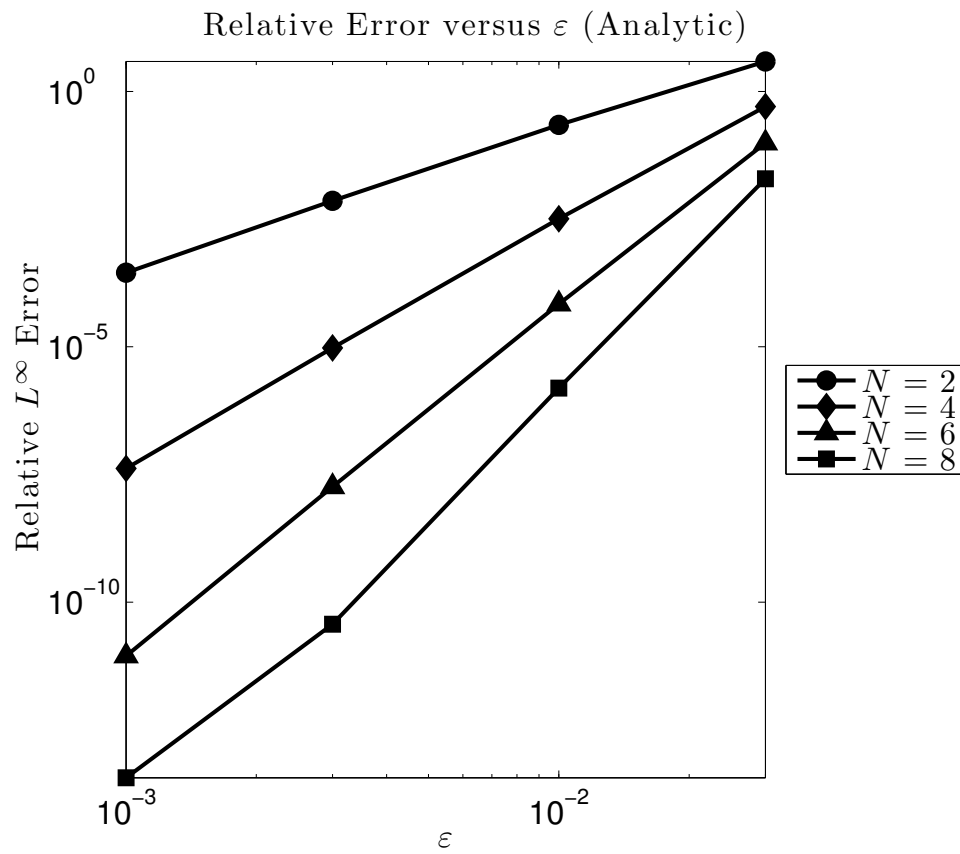


Figure 2. Plot of relative  $L^\infty$  error versus perturbation order  $N$  for the analytic profile, (Equation 1.23b) ( $\varepsilon = 10^{-3}, 3 \times 10^{-3}, 10^{-2}, 3 \times 10^{-2}$ ).

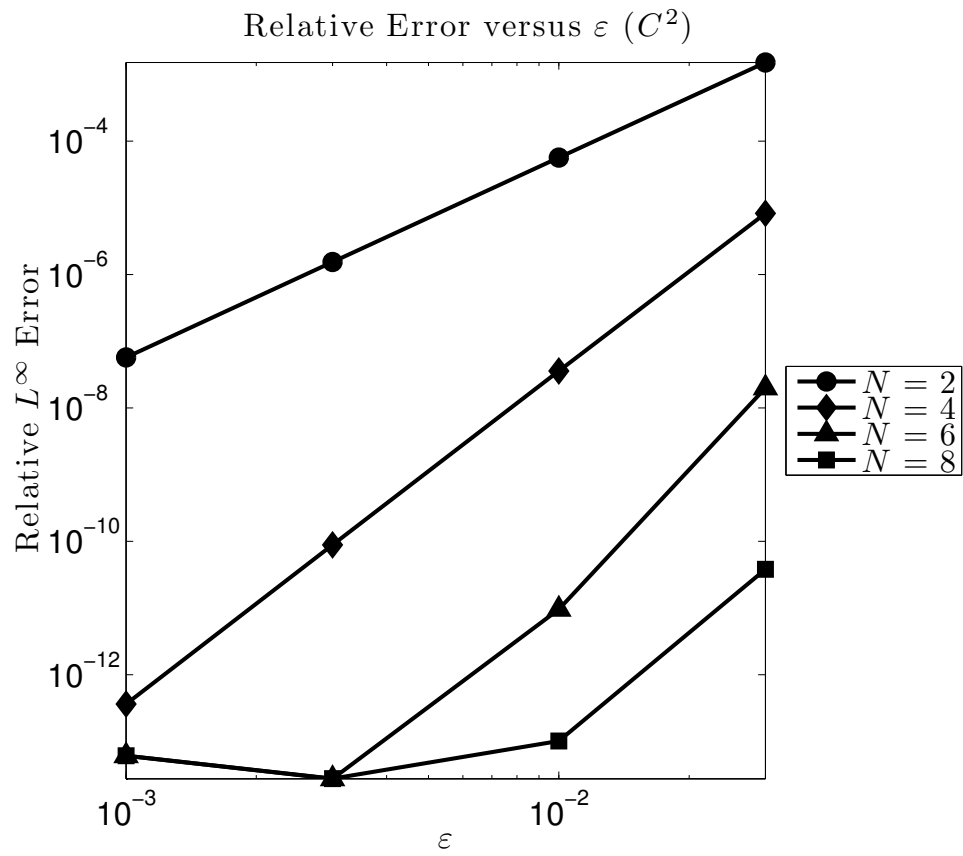


Figure 3. Plot of relative  $L^\infty$  error versus perturbation order  $N$  for the  $C^2$  profile, (Equation 1.23c) ( $\varepsilon = 10^{-3}, 3 \times 10^{-3}, 10^{-2}, 3 \times 10^{-2}$ ).

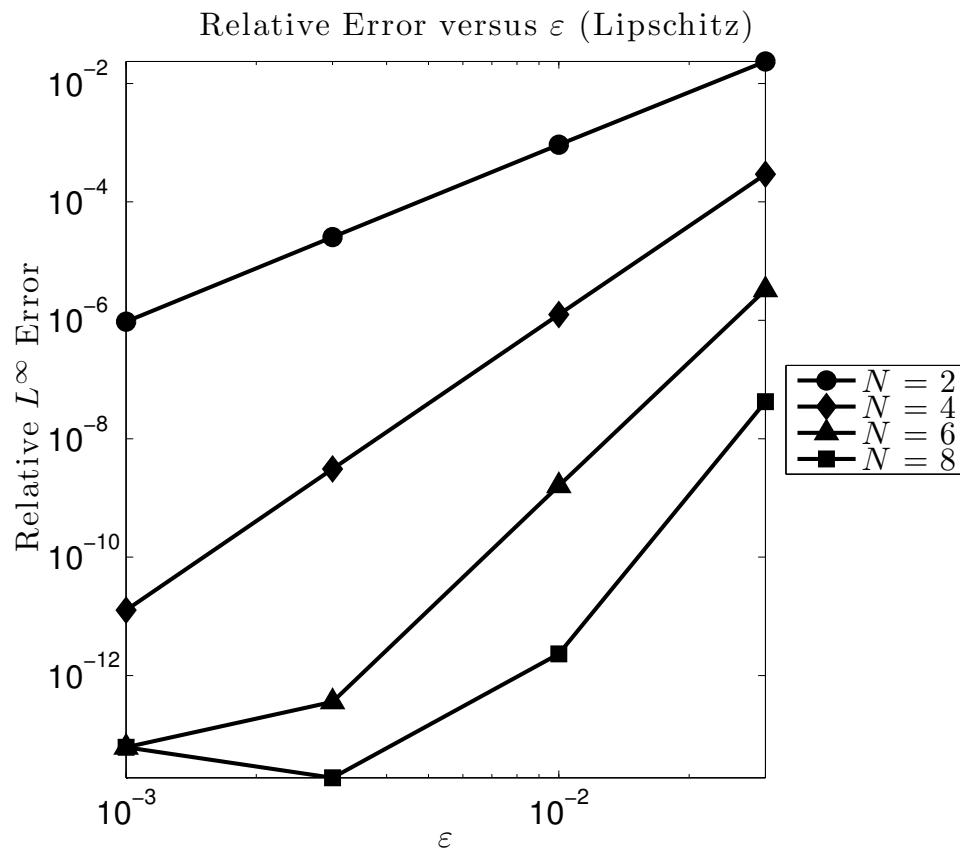


Figure 4. Plot of relative  $L^\infty$  error versus perturbation order  $N$  for the Lipschitz profile, (Equation 1.23d) ( $\varepsilon = 10^{-3}, 3 \times 10^{-3}, 10^{-2}, 3 \times 10^{-2}$ ).

## CHAPTER 2

### INTERFACE RECOVERY

#### 2.1 Introduction

The interior of the earth's crust can effectively be modeled as a layered media: largely homogeneous blocks of material separated by sharp interfaces across which material properties change discontinuously. Two important and related questions are raised naturally by many. (1) Given the knowledge of the material properties of the layers and the shapes of the interfaces, can one compute scattering wave returns from such a structure given incident radiation? (2) Specifying incident radiation and measuring scattered waves, can one deduce information about material properties and interface shapes within the layered media? To address these questions, we first implemented the forward solver designed by Malcolm and Nicholls (63) using FFTW-MPI(64) and OpenMP(65), then we designed a linear inverse solver, which we tested using the data from the forward solver.

##### 2.1.1 Previous Work

From the introduction of the previous chapter, § 1.1, we know that there are many papers on classical numerical methods like the finite difference method, the finite element method, the spectral element method and surface methods, which can be implemented to solve the forward problem. Also there are huge volumes of books and papers ((18) has a good introduction) on methods for the inverse problem.

Here we propose a boundary perturbation method for inverse problems for irregularly shaped periodic layered media. Our approach avoids the need for specialized quadrature rules, and is a generalization of the 'method of operator expansions' (OE) of Milder(30; 42; 43; 44; 45; 46) that we described in chapter § 1 which we use precisely because the interface shapes appear so explicitly in these formulations making them particularly appealing for the development of an inversion algorithm.

Milder showed that OE method is spectrally accurate, which means the numerical convergence rate is faster than any polynomial order. For our method, as the scattered fields is analytic with respect to boundary perturbation and the choice of spatial basis is optimal, it also inherits the spectral accuracy. Our approach is developed based on the work of Malcolm and Nicholls(63) and the work of Nicholls and Taber(66; 67) on interface recovery.

## 2.2 Governing Equation

The domain of interest is a  $(d_1, d_2)$ -periodic structure that contains two layers of medium, where the medium on the top is in domain  $S_u$  and the medium on the bottom is in domain  $S_v$ .

$$\text{Area}_u = \{(x, y, z) | 0 > z > g(x, y)\}$$

$$\text{Area}_v = \{(x, y, z) | z < g(x, y)\}$$

$$g(x + d_1, y) = g(x, y) = g(x, y + d_2), \quad g(x, y) = \bar{g} + \varepsilon f(x, y)$$

The wave scattering not only satisfies the Helmholtz equation with an incident radiation from up the surface, but also OWC at infinity.

The normal on the interface of two medium is

$$\mathbf{N} = (-\partial_x g, -\partial_y g, 1)^T.$$

We assume the density of each domain is constant, thus we can set the velocity of waves propagating in each layer to be  $c_j$  ( $j = u, v$ ); We assume incident radiation of the form

$$\mathbf{u}(x, y, z, t) = e^{-i\omega t} e^{i(\alpha x + \beta y + \gamma_u z)} = e^{-i\omega t} \mathbf{u}_i(x, y, z). \quad (2.1)$$

We also define a parameter  $k_j$  in each layer so that  $k_j = \omega/c_j$ ; It is the magnitude of the wavenumber of interest. e.g. we have

$$\alpha^2 + \beta^2 + \beta_u^2 = k_u^2$$

$$\alpha^2 + \beta^2 + \beta_v^2 = k_v^2$$

From the work of Malcolm and Nicholls (63) and (68), we know that the solutions to the Helmholtz equation are quasiperiodic. If we denote

$$\{\mathbf{u}, \mathbf{v}\} = \{\mathbf{u}(x, y, z), \mathbf{v}(x, y, z)\}$$

then quasi periodicity means

$$u(x + \mathbf{d}, \mathbf{y}, z) = e^{i\alpha \mathbf{d}} u(x, \mathbf{y}, z)$$

$$v(x + \mathbf{d}, \mathbf{y}, z) = e^{i\alpha \mathbf{d}} v(x, \mathbf{y}, z).$$

The equations governing the waves propagating in these media are the well-known Helmholtz equations, with the outgoing wave conditions,

$$\Delta u + k_u^2 u = 0 \quad 0 > z > g(x, \mathbf{y}) \quad (2.1a)$$

$$\mathcal{B}u = 0 \quad \mathbf{y} \rightarrow \infty \quad (2.1b)$$

$$\Delta v + k_v^2 v = 0 \quad z < g(x, \mathbf{y}) \quad (2.1c)$$

$$\mathcal{B}v = 0 \quad \mathbf{y} \rightarrow -\infty \quad (2.1d)$$

$$\mathbf{u} - \mathbf{v} = \boldsymbol{\xi} \quad \partial_{\mathbf{N}}(\mathbf{u} - \mathbf{v}) = \boldsymbol{\psi} \quad \mathbf{y} = g(x, \mathbf{y}) \quad (2.1e)$$

$$\boldsymbol{\xi}(x) := -\mathbf{u}_i(x, \mathbf{y}, g(x, \mathbf{y})) = -e^{i(\alpha x + \beta \mathbf{y} - \gamma_u g(x, \mathbf{y}))} \quad (2.1f)$$

$$\boldsymbol{\psi}(x) := -[\partial_{\mathbf{N}} \mathbf{u}_i(x, \mathbf{y}, z)]_{z=g(x, \mathbf{y})} = (i\gamma_u + i\beta(\partial_{\mathbf{y}} g) + i\alpha(\partial_x g)) e^{i(\alpha x + \beta \mathbf{y} - \gamma_u g(x, \mathbf{y}))}. \quad (2.1g)$$

It is important to understand the 'outgoing wave condition' (OWC) (68) before we proceed.

**Proposition 2.2.1.** *The solutions to (Equation 2.1a) are*

$$\begin{aligned} u(x, y, z) &= \sum_{|p|=-\infty}^{\infty} a_p e^{i(\alpha_p x + \beta_p y + \gamma_{u,p} z)} \quad z > \bar{g} + \varepsilon \cdot |f|_{\infty} \\ v(x, y, z) &= \sum_{|p|=-\infty}^{\infty} b_p e^{i(\alpha_p x + \beta_p y - \gamma_{v,p} z)} \quad z < \bar{g} - \varepsilon \cdot |f|_{\infty} \end{aligned}$$

*based on the quasi periodicity of the solution and outgoing wave condition.*

*Proof.* From the quasi periodicity of the solution, assume  $d$  is the period of the structure, we know that

$$\alpha_p = \alpha + (2\pi/d)p \quad \beta_p = \beta + (2\pi/d)p \quad p \in \mathbb{Z}$$

$$\gamma_{j,p} = \begin{cases} \sqrt{k_j^2 - \alpha_p^2 - \beta_p^2}, & \alpha_p^2 + \beta_p^2 < k_j^2 \\ i \sqrt{\alpha_p^2 + \beta_p^2 - k_j^2}, & \alpha_p^2 + \beta_p^2 > k_j^2 \end{cases}, \quad j = u, v.$$

Then generally the solution  $u(x, y)$  will be

$$u(x, y) = \sum_{|p|=-\infty}^{\infty} a_p e^{i(\alpha_p x + \beta_p y + \gamma_{u,p} z)} + c_p e^{i(\alpha_p x + \beta_p y - \gamma_{u,p} z)}. \quad (2.2)$$

From equation (Equation 2.1b), we know that when  $z$  goes to  $\infty$ ,  $u(x, y, z)$  should decay to zero. When  $p$  is large enough,  $\gamma_{j,p} = i\sqrt{\alpha_p^2 + \beta_p^2 - k_j^2}$ , and

$$-i\gamma_{u,p} z = -i \cdot i \sqrt{\alpha_p^2 + \beta_p^2 - k_j^2} z = \sqrt{\alpha_p^2 + \beta_p^2 - k_j^2} z. \quad (2.3)$$

As  $z$  goes to  $\infty$ , then  $e^{-i\gamma_{v,p}z}$  will also go to  $\infty$ , which will violate equation (Equation 2.1b), thus we have to set  $c_p$  in equation (Equation 2.2) to be 0. Similarly if we set

$$v(x, y, z) = \sum_{|p|=-\infty}^{\infty} b_p e^{i(\alpha_p x + \beta_p y - \gamma_{v,p} z)} + d_p e^{i(\alpha_p x + \beta_p y + \gamma_{v,p} z)} \quad (2.4)$$

we can also prove  $d_p$  in equation (Equation 2.4) must be zero, as  $e^{i\gamma_{v,p}z}$  goes to  $\infty$  when  $p$  is large enough and  $z$  goes to  $-\infty$ .  $\square$

### 2.3 Forward Problem

For the forward problem, the shape of the grating  $g(x, y)$  is given, and the Dirichlet data  $\zeta(x, y)$  and Neumann data  $\psi(x, y)$  are derived from the incident radiation. Thus, we should be able to solve for the scattered fields  $u(x, y, z)$ , and  $v(x, y, z)$ , in particular  $u(x, y, 0)$ . Using notation  $\mathbf{N} = (-\partial_x g(x, y), -\partial_y g(x, y), 1)$ , and defining:

$$\mathbf{U}(x, y) := u(x, y, g(x, y)), \quad \mathbf{V}(x, y) := v(x, y, g(x, y)) \quad (2.5)$$

$$\mathbf{U}'(x, y) := \partial_{\mathbf{N}} u(x, y, g(x, y)), \quad \mathbf{V}'(x, y) := \partial_{\mathbf{N}} v(x, y, g(x, y)) \quad (2.6)$$

$$\mathbf{G}(g)[\mathbf{U}(x, y)] := \mathbf{U}'(x, y), \quad \mathbf{H}(g)[\mathbf{V}(x, y)] := \mathbf{V}'(x, y) \quad (2.7)$$

Where  $\mathbf{G}$  and  $\mathbf{H}$  are the DNOs. From the boundary conditions, we obtain:

$$\mathbf{U} - \mathbf{V} = \zeta \quad (2.8)$$

$$G[\mathbf{U}] - H[\mathbf{V}] = \psi \quad (2.9)$$

$$u(x, y, 0) =: P[\mathbf{U}] \quad (2.10)$$

Where operator  $P$  from (Equation 2.10) is called the Upward Propagator which maps the scattered wave on the interface  $z = g(x, y)$  to the above surface  $z = 0$ . We will discuss how to solve this operator in section § 2.3.2.

We can solve (Equation 2.8) for  $\mathbf{V}$  and get  $\mathbf{V} = \mathbf{U} - \zeta$ , then plugging it into (Equation 2.9) we get

$$G[\mathbf{U}] - H[\mathbf{U} - \zeta] = \psi$$

which implies:

$$(G - H)[\mathbf{U}] = \psi - H[\zeta]$$

Thus for a known interface  $z = g(x, y)$ , as long as we know how to calculate the operators  $G, H$  we can get  $\mathbf{U}$ , and then by (Equation 2.10) we can solve for  $u(x, y, 0)$  after having a good understanding of operator  $P$ .

### 2.3.1 Surface Data Expansions

We represent the Dirichlet and Neumann data as expansions in the grating height/slope.

We start with  $\zeta$ :

$$\zeta(x, y; \varepsilon) = \sum_{n=0}^{\infty} \zeta_n(x, y) \varepsilon^n.$$

On the other hand, we know that

$$\begin{aligned}\zeta(x, y; \varepsilon) &= -e^{i(\alpha x + \beta y - \gamma_u(\bar{g} + \varepsilon f(x, y)))} \\ &= -e^{i(\alpha x + \beta y)} e^{-i\gamma_u \bar{g}} \sum_{n=0}^{\infty} F_n(x, y) (-i\gamma_u)^n \varepsilon^n,\end{aligned}$$

where

$$g(x, y) = \bar{g} + \varepsilon f(x, y)$$

$$F_n(x, y) := f^n(x, y)/(n!).$$

Thus by equating corresponding orders in both expressions we can prove that:

$$\zeta_n = -e^{i(\alpha x + \beta y)} e^{-i\gamma_u \bar{g}} F_n(x, y) (-i\gamma_u)^n. \quad (2.11)$$

Then we can apply similar ideas to find the different orders of  $\psi$ . We have

$$\begin{aligned}
\psi(x, y; \varepsilon) &= \sum_{n=0}^{\infty} \psi_n(x, y) \varepsilon^n \\
&= \partial_N \zeta(x, y; \varepsilon) \\
&= -(-\partial_x g, -\partial_y g, 1) \cdot (i\alpha, i\beta, -i\gamma_u) (e^{i(\alpha x + \beta y - \gamma_u(\bar{g} + \varepsilon f(x, y)))}) \\
&= (i\gamma_u + i\alpha\varepsilon(\partial_x f) + i\beta\varepsilon(\partial_y f)) \left( e^{i(\alpha x + \beta y)} e^{-i\gamma_u \bar{g}} \sum_{n=0}^{\infty} F_n(x, y) (-i\gamma_u)^n \varepsilon^n \right) \\
&= e^{i(\alpha x + \beta y)} e^{-i\gamma_u \bar{g}} \left( i\gamma_u \sum_{n=1}^{\infty} F_n(x, y) (-i\gamma_u)^n \varepsilon^n + (i\alpha\partial_x f + i\beta\partial_y f) \sum_{n=0}^{\infty} F_n(x, y) (-i\gamma_u)^n \varepsilon^n \right) \\
&= e^{i(\alpha x + \beta y)} e^{-i\gamma_u \bar{g}} \left( -\sum_{n=0}^{\infty} F_n(x, y) (-i\gamma_u)^{n+1} \varepsilon^n + \sum_{n=1}^{\infty} (i\alpha\partial_x f + i\beta\partial_y f) F_{n-1}(x, y) (-i\gamma_u)^{n-1} \varepsilon^n \right)
\end{aligned}$$

By equating both sides of the equation, we can observe that

$$\psi_0 = (i\gamma_u) e^{-i\gamma_u \bar{g}} e^{i(\alpha x + \beta y)} \quad (2.11b)$$

$$\psi_n = \left( -F_n(x, y) (-i\gamma_u)^{n+1} + ((i\alpha)(\partial_x f) + i\beta(\partial_y f)) F_{n-1}(x, y) (-i\gamma_u)^{n-1} \right) e^{-i\gamma_u \bar{g}} e^{i(\alpha x + \beta y)}. \quad (2.11b)$$

### 2.3.2 Operator Expansions of the Upward Propagator

Now to understand the behavior of operator  $P$ , we need to understand how it acts on Fourier basis functions, then we will know its operation on any periodic  $L^2$  functions. As we

have seen in (Equation 2.10), the Upward propagator  $P$  maps the surface data  $U$  to the upper field  $\tilde{u} = u(x, y, 0)$ . Consider

$$u_p(x, y, z) = e^{i(\alpha_p x + \beta_p y - \gamma_{u,p} z)},$$

which is a solution to our governing equation and satisfies the OWC. Thus from (Equation 2.10), we get

$$P(g)[u_p(x, y, g(x, y))] = u_p(x, y, 0)$$

which implies:

$$P(g)[e^{i(\alpha_p x + \beta_p y - \gamma_{u,p} g(x, y))}] = e^{i(\alpha_p x + \beta_p y)}. \quad (2.12)$$

**Proposition 2.3.1.** *The Upward propagator  $P$  satisfies*

$$P_0[\xi] = e^{-i\gamma_{u,D} \bar{g} \xi} \quad (2.12a)$$

$$P_n[\xi] = - \sum_{m=0}^{n-1} P_m[F_{n-m}(x, y)(i\gamma_{u,D})^{n-m} \xi] \quad (2.12b)$$

*given that*

$$g(x, y) = \bar{g} + \varepsilon f(x, y)$$

*Proof.* Note that

$$P(g) = \sum_{n=0}^{\infty} P_n(g) \varepsilon^n$$

Thus from (Equation 2.12) we know that

$$\left( \sum_{n=0}^{\infty} P_n(g) \varepsilon^n \right) \left( e^{i(\alpha_p x + \beta_p y)} e^{i\gamma_{u,p}} \sum_{n=0}^{\infty} F_n(x, y) (i\gamma_{u,p})^n \varepsilon^n \right) = e^{i(\alpha_p x + \beta_p y)}$$

Now we first study the zeroth order and we find that

$$P_0(e^{i(\alpha_p x + \beta_p y)} e^{i\gamma_{u,p} \bar{g}}) = e^{i(\alpha_p x + \beta_p y)}$$

implying

$$P_0(e^{i(\alpha_p x + \beta_p y)}) = e^{-i\gamma_{u,p} \bar{g}} e^{i(\alpha_p x + \beta_p y)}$$

which gives

$$P_0[\xi] = e^{-i\gamma_{u,D} \bar{g}} \xi.$$

Note here we used a Fourier multiplier

$$m(D)[\xi] := \sum_{p=-\infty}^{\infty} m(p) \hat{\xi}_p e^{i(\alpha_p x + \beta_p y)}.$$

If we equate the  $n$ -th order where  $n > 0$ , then it follows that

$$\begin{aligned} \sum_{m=0}^n P_m [F_{n-m}(x, y) (i\gamma_{u,p})^{n-m} e^{i\gamma_{u,p}\bar{g}} e^{i(\alpha_p x + \beta_p y)}] &= 0, \\ P_n [e^{i\gamma_{u,p}\bar{g}} e^{i(\alpha_p x + \beta_p y)}] &= - \sum_{m=0}^{n-1} P_m [F_{n-m}(x, y) (i\gamma_{u,p})^{n-m} e^{i\gamma_{u,p}\bar{g}} e^{i(\alpha_p x + \beta_p y)}], \\ P_n [e^{i(\alpha_p x + \beta_p y)}] &= - \sum_{m=0}^{n-1} P_m [F_{n-m}(x, y) (i\gamma_{u,p})^{n-m} e^{i(\alpha_p x + \beta_p y)}], \\ P_n [\xi] &= - \sum_{m=0}^{n-1} P_m [F_{n-m}(x, y) (i\gamma_{u,D})^{n-m} \xi]. \end{aligned}$$

□

**Remark 2.3.2.** If we study the operator  $P$ , we can see that when  $p$  is small enough, e.g. when

$$\alpha_p^2 + \beta_p^2 < k_u^2,$$

then  $\gamma_{u,p}$  will be a positive number (propagating mode), and the Fourier multiplier  $e^{i\gamma_{u,p}\bar{g}}$  is of modulus one. But if  $p$  is large so that

$$\alpha_p^2 + \beta_p^2 > k_u^2,$$

which is an evanescent mode of  $p$ , according to (Equation 2.3) and the fact that  $\bar{g} < 0$ , we find that the Fourier multiplier  $e^{-i\gamma_{u,D}\bar{g}}$  will be exponentially decaying, so the upward propagator is very nice and smooth for the forward problem. But in terms of the inverse solver in § 2.4,

we need to use the operator  $P_0^{-1}$  which will, on the other hand, enlarge the Fourier coefficients exponentially when  $p$  is large.

### 2.3.3 Operator Expansions of the Dirichlet-Neumann Operators

We now first focus on the DNO  $G$  that generates normal derivative  $U'$  from Dirichlet data  $U$  on the surface  $g(x, y) = \varepsilon f(x, y)$ . We define

$$u_p(x, y, z) = e^{i(\alpha_p x + \beta_p y + \gamma_{u,p} z)}$$

By the definition of operator  $G$  (Equation 2.7), we have

$$\begin{aligned} G(g)[u_p(x, y, g(x, y))] &= \partial_N u_p \\ &= (i\alpha_p, i\beta_p, i\gamma_{u,p}) \cdot (-\partial_x g, -\partial_y g, 1) u_p(x, y, g(x, y)) \\ &= (-i\alpha_p \partial_x g - i\beta_p \partial_y g + i\gamma_{u,p}) u_p(x, y, g(x, y)). \end{aligned}$$

Also we have expansions of  $G$  and  $u_p(x, y, g(x, y))$  as follows:

$$G = \sum_{n=0}^{\infty} G_n \varepsilon^n,$$

and

$$\begin{aligned}
u_p(x, y, g(x, y)) &= e^{i(\alpha_p x + \beta_p y + \gamma_{u,p} g(x, y))} \\
&= e^{i(\alpha_p x + \beta_p y)} e^{i\gamma_{u,p} g(x, y)} \\
&= e^{i(\alpha_p x + \beta_p y)} \sum_{n=0}^{\infty} (i\gamma_{u,p})^n F_n(x, y) \varepsilon^n.
\end{aligned}$$

Then by substituting the above two expansions into the definition of operator  $G$ , we get the left hand side as follows,

$$\begin{aligned}
G(g)[u_p(x, y, g(x, y))] &= \left( \sum_{n=0}^{\infty} G_n \varepsilon^n \right) \left( e^{i(\alpha_p x + \beta_p y)} \cdot \sum_{n=0}^{\infty} (i\gamma_{u,p})^n F_n(x, y) \varepsilon^n \right) \\
&= \sum_{n=0}^{\infty} \sum_{m=0}^n G_m \left[ F_{n-m} (i\gamma_{u,p})^{n-m} e^{i(\alpha_p x + \beta_p y)} \right] \varepsilon^n.
\end{aligned}$$

The expansion of right hand side becomes the following:

$$\begin{aligned}
&(-i\alpha_p \partial_x g - i\beta_p \partial_y g + i\gamma_{u,p}) u_p(x, y, g(x, y)) \\
&= (-i\alpha_p (\partial_x f) \varepsilon - i\beta_p (\partial_y f) \varepsilon + i\gamma_{u,p}) e^{i(\alpha_p x + \beta_p y)} \sum_{n=0}^{\infty} (i\gamma_{u,p})^n F_n(x, y) \varepsilon^n \\
&= \left( - \sum_{n=0}^{\infty} (i\alpha_p \partial_x f + i\beta_p \partial_y f) F_n(x, y) (i\gamma_{u,p})^n \varepsilon^{n+1} + \sum_{n=0}^{\infty} F_n(x, y) (i\gamma_{u,p})^{n+1} \varepsilon^n \right) e^{i(\alpha_p x + \beta_p y)} \\
&= \left( - \sum_{n=1}^{\infty} (i\alpha_p \partial_x f + i\beta_p \partial_y f) F_{n-1}(x, y) (i\gamma_{u,p})^{n-1} \varepsilon^n + \sum_{n=0}^{\infty} F_n(x, y) (i\gamma_{u,p})^{n+1} \varepsilon^n \right) e^{i(\alpha_p x + \beta_p y)} \\
&= \left( - \sum_{n=1}^{\infty} (i\alpha_p \partial_x F_n + i\beta_p \partial_y F_n) (i\gamma_{u,p})^{n-1} \varepsilon^n + \sum_{n=0}^{\infty} F_n(x, y) (i\gamma_{u,p})^{n+1} \varepsilon^n \right) e^{i(\alpha_p x + \beta_p y)}.
\end{aligned}$$

Note we used the facts that

$$\partial_x F_n(x, y) = \partial_x f(x, y) F_{n-1}(x, y), \quad \partial_y F_n(x, y) = \partial_y f(x, y) F_{n-1}(x, y).$$

**Proposition 2.3.3.** *The DNO  $G$  operator satisfies*

$$G_0[\xi] = (i\gamma_{u,D})\xi, \tag{2.13}$$

and

$$\begin{aligned} G_n[\xi] = & -k_u^2 F_n(i\gamma_{u,D})^{n-1} \xi - \partial_x \left[ F_n \partial_x (i\gamma_{u,D})^{n-1} \xi \right] \\ & - \partial_y \left[ F_n \partial_y (i\gamma_{u,D})^{n-1} \xi \right] - \sum_{m=0}^{n-1} G_m \left[ F_{n-m} (i\gamma_{u,D})^{n-m} \xi \right]. \end{aligned} \tag{2.14}$$

*Proof.* Referring to the expansions of the left hand side and right hand side of (Equation 2.7),

for zeroth order equality it holds that

$$\begin{aligned} G_0[e^{i(\alpha_p x + \beta_p y)}] &= F_0(x, y) (i\gamma_{u,p})^{0+1} e^{i(\alpha_p x + \beta_p y)} \\ &= (i\gamma_{u,p}) e^{i(\alpha_p x + \beta_p y)}, \end{aligned}$$

e.g.  $G_0[\xi] = (i\gamma_{u,D})[\xi]$  in the sense of Fourier multipliers. After equating n-th order on both sides of the expansions, we get

$$\begin{aligned}
& \sum_{m=0}^n G_m[F_{n-m}(i\gamma_{u,p})^{n-m} e^{i(\alpha_p x + \beta_p y)}] \\
&= -(i\alpha_p \partial_x F_n + i\beta_p \partial_y F_n)(i\gamma_{u,p})^{n-1} e^{i(\alpha_p x + \beta_p y)} + F_n(i\gamma_{u,p})^{n+1} e^{i(\alpha_p x + \beta_p y)} \\
&= \left( -i\alpha_p \partial_x F_n - i\beta_p \partial_y F_n + F_n(i\gamma_{u,p})^2 \right) (i\gamma_{u,p})^{n-1} e^{i(\alpha_p x + \beta_p y)} \\
&= \left( -i\alpha_p \partial_x F_n - i\beta_p \partial_y F_n + F_n \left( -k_u^2 - (i\alpha_p)^2 - (i\beta_p)^2 \right) \right) (i\gamma_{u,p})^{n-1} e^{i(\alpha_p x + \beta_p y)} \\
&= - \left( (\partial_x F_n + F_n(i\alpha_p))(i\alpha_p) + (\partial_y F_n + F_n(i\beta_p))(i\beta_p) + k_u^2 F_n \right) (i\gamma_{u,p})^{n-1} e^{i(\alpha_p x + \beta_p y)} \\
&= -\partial_x \left[ F_n \partial_x (i\gamma_{u,p})^{n-1} e^{i(\alpha_p x + \beta_p y)} \right] - \partial_y \left[ F_n \partial_y (i\gamma_{u,p})^{n-1} e^{i(\alpha_p x + \beta_p y)} \right] \\
&\quad - k_u^2 F_n (i\gamma_{u,p})^{n-1} e^{i(\alpha_p x + \beta_p y)}.
\end{aligned}$$

Using Fourier multiplier notation, we can translate the result into

$$\begin{aligned}
\sum_{m=0}^n G_m[F_{n-m}(i\gamma_{u,D})^{n-m} \xi] &= -\partial_x \left[ F_n \partial_x (i\gamma_{u,D})^{n-1} \xi \right] - \partial_y \left[ F_n \partial_y (i\gamma_{u,D})^{n-1} \xi \right] \\
&\quad - k_u^2 F_n (i\gamma_{u,D})^{n-1} \xi. \quad (2.15)
\end{aligned}$$

If we isolate the term  $G_n[\xi]$  on the LHS, we have proven the result,

$$\begin{aligned}
G_n[\xi] &= -k_u^2 F_n (i\gamma_{u,D})^{n-1} \xi - \partial_x \left[ F_n \partial_x (i\gamma_{u,D})^{n-1} \xi \right] \\
&\quad - \partial_y \left[ F_n \partial_y (i\gamma_{u,D})^{n-1} \xi \right] - \sum_{m=0}^{n-1} G_m \left[ F_{n-m} (i\gamma_{u,D})^{n-m} \xi \right].
\end{aligned}$$

□

Particularly, we will need to use the result when  $n = 1$  in section § 2.4, i.e.

$$\begin{aligned} G_1[\xi] &= -k_u^2 f \xi - \partial_x [f \partial_x \xi] - \partial_y [f \partial_y \xi] - G_0 [f(i\gamma_{u,p}) \xi] \\ &= -k_u^2 f \xi - \partial_x [f \partial_x \xi] - \partial_y [f \partial_y \xi] - G_0 [f G_0[\xi]]. \end{aligned}$$

Now we proceed to the DNO H that generates the normal derivative  $V'$  from Dirichlet data  $V$  on the surface. We set

$$v_p(x, y, z) = e^{i(\alpha_p x + \beta_p y - \gamma_{v,p} z)},$$

and as we have proven for  $u_p(x, y, z)$ , it also holds for  $v_p(x, y, z)$  that it satisfies the Helmholtz equation and the outgoing wave condition in the area  $g(x, y) > z > -\infty$ . Now, we derive the exact form of all orders of the DNO H. By the definition of operator H (Equation 2.7), we have

$$\begin{aligned} H(g)[v_p(x, y, g(x, y))] &= \partial_N v_p \\ &= (-\partial_x g, -\partial_y g, 1) \cdot (i\alpha_p, i\beta_p, -i\gamma_{v,p}) v_p(x, y, g(x, y)) \\ &= -((i\alpha_p)\partial_x g + (i\beta_p)\partial_y g + i\gamma_{v,p}) v_p(x, y, g(x, y)). \end{aligned}$$

Expanding H and  $v_p(x, y, g(x, y))$ , we get

$$H = \sum_{n=0}^{\infty} H_n \varepsilon^n,$$

and

$$\begin{aligned}
v_p(x, y, g(x, y)) &= e^{i(\alpha_p x + \beta_p y - \gamma_{v,p} g(x, y))} \\
&= e^{i(\alpha_p x + \beta_p y)} e^{-i\gamma_{v,p} g(x, y)} \\
&= e^{i(\alpha_p x + \beta_p y)} \sum_{n=0}^{\infty} (-i\gamma_{v,p})^n F_n(x, y) \varepsilon^n.
\end{aligned}$$

Substituting the above two expansions into the definition of operator H (Equation 2.7), the LHS becomes

$$\begin{aligned}
H(g)[v_p(x, y, g(x, y))] &= \left( \sum_{n=0}^{\infty} H_n \varepsilon^n \right) \left( e^{i(\alpha_p x + \beta_p y)} \sum_{n=0}^{\infty} (-i\gamma_{v,p})^n F_n(x, y) \varepsilon^n \right) \\
&= \sum_{n=0}^{\infty} \sum_{m=0}^n H_m \left[ F_{n-m} (-i\gamma_{v,p})^{n-m} e^{i(\alpha_p x + \beta_p y)} \right] \varepsilon^n.
\end{aligned}$$

The expansions of the right hand side are,

$$\begin{aligned}
& - (i\alpha_p \partial_x g + i\beta_p \partial_y g + i\gamma_{v,p}) v_p(x, y, g(x, y)) \\
&= - (i\alpha_p (\partial_x f) \varepsilon + i\beta_p (\partial_y f) \varepsilon + i\gamma_{v,p}) \cdot e^{i(\alpha_p x + \beta_p y)} \cdot \sum_{n=0}^{\infty} (-i\gamma_{v,p})^n F_n(x, y) \varepsilon^n \\
&= - \left( \sum_{n=0}^{\infty} (i\alpha_p \partial_x f + i\beta_p \partial_y f) F_n(x, y) (-i\gamma_{v,p})^n \varepsilon^{n+1} - \sum_{n=0}^{\infty} F_n(x, y) (-i\gamma_{v,p})^{n+1} \varepsilon^n \right) e^{i(\alpha_p x + \beta_p y)} \\
&= \left( - \sum_{n=1}^{\infty} (i\alpha_p \partial_x f + i\beta_p \partial_y f) F_{n-1}(x, y) (-i\gamma_{v,p})^{n-1} \varepsilon^n + \sum_{n=0}^{\infty} F_n(x, y) (-i\gamma_{v,p})^{n+1} \varepsilon^n \right) e^{i(\alpha_p x + \beta_p y)} \\
&= \left( - \sum_{n=1}^{\infty} (i\alpha_p \partial_x F_n + i\beta_p \partial_y F_n) (-i\gamma_{v,p})^{n-1} \varepsilon^n + \sum_{n=0}^{\infty} F_n(x, y) (-i\gamma_{v,p})^{n+1} \varepsilon^n \right) e^{i(\alpha_p x + \beta_p y)}.
\end{aligned}$$

**Proposition 2.3.4.** *The DNO  $H$  operator satisfies*

$$H_0[\xi] = (-i\gamma_{v,D})\xi, \quad (2.16)$$

and

$$\begin{aligned} H_n[\xi] = & -k_v^2 F_n (-i\gamma_{v,D})^{n-1} \xi - \partial_x \left[ F_n \partial_x (-i\gamma_{v,D})^{n-1} \xi \right] \\ & - \partial_y \left[ F_n \partial_y (-i\gamma_{v,D})^{n-1} \xi \right] - \sum_{m=0}^{n-1} H_m \left[ F_{n-m} (-i\gamma_{v,D})^{n-m} \xi \right]. \end{aligned} \quad (2.17)$$

*Proof.* Referring to the expansions of LHS and RHS of (Equation 2.7), for zeroth order equality it holds that

$$\begin{aligned} H_0[e^{i(\alpha_p x + \beta_p y)}] &= F_0(x, y) (-i\gamma_{v,p})^{0+1} e^{i(\alpha_p x + \beta_p y)} \\ &= (-i\gamma_{v,p}) e^{i(\alpha_p x + \beta_p y)}, \end{aligned}$$

e.g.  $H_0[\xi] = (-i\gamma_{v,D})[\xi]$  in the sense of Fourier multipliers. After equating n-th order on both sides of the expansions, we get

$$\begin{aligned}
& \sum_{m=0}^n H_m[F_{n-m}(-i\gamma_{v,p})^{n-m} e^{i(\alpha_p x + \beta_p y)}] \\
&= -(i\alpha_p \partial_x F_n + i\beta_p \partial_y F_n)(-i\gamma_{v,p})^{n-1} e^{i(\alpha_p x + \beta_p y)} + F_n(-i\gamma_{v,p})^{n+1} e^{i(\alpha_p x + \beta_p y)} \\
&= \left( -i\alpha_p \partial_x F_n - i\beta_p \partial_y F_n + F_n(-i\gamma_{v,p})^2 \right) (i\gamma_{v,p})^{n-1} e^{i(\alpha_p x + \beta_p y)} \\
&= \left( -i\alpha_p \partial_x F_n - i\beta_p \partial_y F_n + F_n \left( -k_v^2 - (i\alpha_p)^2 - (i\beta_p)^2 \right) \right) (-i\gamma_{v,p})^{n-1} e^{i(\alpha_p x + \beta_p y)} \\
&= - \left( (\partial_x F_n + F_n(i\alpha_p))(i\alpha_p) + (\partial_y F_n + F_n(i\beta_p))(i\beta_p) + k_v^2 F_n \right) (-i\gamma_{v,p})^{n-1} e^{i(\alpha_p x + \beta_p y)} \\
&= -\partial_x \left[ F_n \partial_x (-i\gamma_{v,p})^{n-1} e^{i(\alpha_p x + \beta_p y)} \right] - \partial_y \left[ F_n \partial_y (-i\gamma_{v,p})^{n-1} e^{i(\alpha_p x + \beta_p y)} \right] \\
&\quad - k_v^2 F_n (-i\gamma_{v,p})^{n-1} e^{i(\alpha_p x + \beta_p y)}.
\end{aligned}$$

Using Fourier multipliers, we can translate the result into

$$\begin{aligned}
\sum_{m=0}^n H_m[F_{n-m}(-i\gamma_{v,D})^{n-m} \xi] &= -\partial_x \left[ F_n \partial_x (-i\gamma_{v,D})^{n-1} \xi \right] - \partial_y \left[ F_n \partial_y (-i\gamma_{v,D})^{n-1} \xi \right] \\
&\quad - k_v^2 F_n (-i\gamma_{v,D})^{n-1} \xi. \quad (2.18)
\end{aligned}$$

If we isolate the term  $H_n[\xi]$  on the LHS, we have proven the result,

$$\begin{aligned}
H_n[\xi] &= -k_v^2 F_n (-i\gamma_{v,D})^{n-1} \xi - \partial_x \left[ F_n \partial_x (-i\gamma_{v,D})^{n-1} \xi \right] \\
&\quad - \partial_y \left[ F_n \partial_y (-i\gamma_{v,D})^{n-1} \xi \right] - \sum_{m=0}^{n-1} H_m \left[ F_{n-m} (-i\gamma_{v,D})^{n-m} \xi \right].
\end{aligned}$$

□

Particularly, we will need to use the result when  $n = 1$  in section § 2.4, i.e.

$$\begin{aligned} H_1[\xi] &= -k_v^2 f \xi - \partial_x [f \partial_x \xi] - \partial_y [f \partial_y \xi] - H_0 [f(-i\gamma_{v,p}) \xi] \\ &= -k_v^2 f \xi - \partial_x [f \partial_x \xi] - \partial_y [f \partial_y \xi] - H_0 [f H_0[\xi]]. \end{aligned}$$

### 2.3.4 Parallel Computing Results for Forward Solver using OpenMP

We have implemented this algorithm in parallel using OpenMP (65), in which we parallelized all sequential processes except Fast Fourier Transforms. We begin with a 2 dimensional solver, and the basic parameters for our experiments are given in Table II.

TABLE II

PARAMETERS USED FOR THE FORWARD SOLVER SIMULATIONS(OPENMP)

Parameter	value	meaning
d	$2\pi$	The period of the grating
$\beta$	5.5	the magnitude of wave number
$\bar{g}$	-1.5	the depth of the interface
$\epsilon$	0.02	the profile heights
f	$\cos(x)$	shape of the interface
N	2400	perturbation orders
nx	12800	number of sub-intervals in x direction

Note here that the forward solver takes as inputs the exactly position  $\bar{g}$  and shape  $\epsilon f(x)$  of the interface, the perturbation order, and the exact value of the incident radiation. It outputs the value of the DNO operator up to order  $N$ .

The following table lists the running time for the sequential code versus an OpenMP implementation with different numbers of threads.

TABLE III

SEQUENTIAL VS OPENMP PERFORMANCE (UNIT : SECONDS)

cases	real time	user time	system time	speedup
sequential	20.405	18.007	2.394	0
openmp 2 threads	14.645	26.280	2.560	0.3933
openmp 4 threads	11.028	40.123	2.619	0.8503
openmp 8 threads	9.333	68.347	3.059	1.186

Table III contains information about the running time, which is the elapsed real time between invocation and termination, and user time, which is the user CPU time.

We can see from Figure 5 that the real time elapsed decreases as we add more threads. This is because the computation jobs are distributed to multiple threads.

In Figure 6 we can see the speedup of computation contributed by using multi-threads.

From Figure 7 we realize that when we use different numbers of threads, the speedup per thread also varies. When the number of threads is 4 we have the maximum speedup per thread, which is 0.2126, i.e. each thread will contribute to 21% speed up.

Lastly, we should note that OpenMP parallel computing is not complete, as Fast Fourier Transforms cannot be parallelized using OpenMP. However we can parallelize all remaining parts.

### **2.3.5 Parallel Computing Results for Forward Solver using FFTW MPI**

From § 2.3.4 we can see that the speedup contributed by each new thread is not very high. In fact using OpenMP, we can only parallelize a small portion of the DNO calculations. Most of the calculation is focused on the Fast Fourier Transform, but OpenMP cannot be used to accelerate FFT, as the Fourier coefficients at different places needs to communicate with each other when a FFT is processed. So in order to increase the speedup per thread, we need to find a way to parallelize the FFT. We used the FFTW MPI package (64) to implement a parallel version of Operator Expansions algorithm (“FFTW won the J. H. Wilkinson Prize for Numerical Software in 1999. The J. H. Wilkinson Prize for Numerical Software is awarded every four years to honor outstanding contributions in the field of numerical software”).

Here are the parameters we used for our experiments.

TABLE IV  
COMMON PARAMETERS USED FOR FORWARD SOLVER NUMERICAL  
SIMULATIONS(MPI)

Parameter	value	meaning
d1	0.53	the period of the grating in x dimension
d2	0.53	the period of the grating in y dimension
$N_h$	100	number of profile heights
h	0:0.001:0.1	profile heights
$\lambda$	0.5	wavelength
$\bar{g}$	-1.5	the depth of the interface
f	$\cos(x)$	shape of the interface
N	32	perturbation orders
nx1	128	number of grid points in x direction
nx2	128	number of grid points in y direction

Note that the computational complexity of the 3D forward solver is much higher than 2D solver, thus we refine grid much less than the 2D solver.

Table V lists the running times for sequential code versus FFTW-MPI with different number of threads.

TABLE V

SEQUENTIAL VS FFTW-MPI PERFORMANCE (UNIT : SECONDS)

cases	real time	user time	system time	speedup
sequential	282.54	152.06	120.42	0
MPI 2 threads	253.51	225.74	259.45	0.115
MPI 4 threads	131.28	345.92	46.62	1.15
MPI 8 threads	94.5	420.35	59.67	1.99

From Table V we notice that, by using only 4 processes, the FFTW-MPI implementation can achieve the same speedup as OpenMP using 8 threads, which shows obvious outperformance to OpenMP, and the speedup contributed by each processes is about **28.8%** when using 4 MPI nodes.

The real time cost and speedup per thread is shown in Figure 8 and Figure 9

## 2.4 Inverse Problem

Our final project involves designing an algorithm to reconstruct the shape of the interface  $g(x)$  from the incident radiation and scattered wave data. The problem is very hard due to the ill-posedness of this inverse problem. But we first decrease the difficulty by specifying more information rather than just the surface data. We will specify the medium properties as well as  $\bar{g}$ , which is the average depth of the layer interface. Then we can focus on the reconstructing of the shape of interface. Currently we have results for a 2 dimensional model.

### 2.4.1 2D Linear Model

In the 2D forward solver, we assume the interface is  $g(x) = \varepsilon f(x)$ , and we have information about the scattered wave on the surface  $y = 0$ . We assume this data to be

$$\eta(x) = u(x, 0),$$

and expanding it in  $\varepsilon$  up to the first order, we have

$$\eta(x) = \eta_0(x) + \eta_1(x) + \mathcal{O}(\varepsilon^2).$$

Equating at like orders, we get

$$\eta_0(x) = u_0(x, 0) \quad \eta_1(x) = u_1(x, 0).$$

However we only know  $\eta(x)$ , not  $\eta_0(x)$  or  $\eta_1(x)$ .

To start, we refer to (Equation 2.9) and (Equation 2.10), and, by the Operator Expansion formulas, we get at zeroth order:

$$P_0 \mathcal{U}_0 = u_0(x, 0) = \eta_0(x)$$

$$(G_0 - H_0) \mathcal{U}_0 = \psi_0 - H_0(\xi_0).$$

To make this more clear, we notice that there are two variables:  $(\eta_0(\mathbf{x})$  and  $\mathbf{U}_0)$  and two equations,

$$\begin{pmatrix} P_0 & -I \\ G_0 - H_0 & 0 \end{pmatrix} \begin{pmatrix} \mathbf{U}_0 \\ \eta_0(\mathbf{x}) \end{pmatrix} = \begin{pmatrix} 0 \\ \psi_0 - H_0(\xi_0) \end{pmatrix}.$$

So  $\mathbf{U}_0$  and  $\eta_0(\mathbf{x})$  can be solved correctly(uniquely), moreover, we can solve for  $\eta_1(\mathbf{x})$  with accuracy within  $\varepsilon^2$  as  $\eta_1(\mathbf{x}) = \eta(\mathbf{x}) - \eta_0(\mathbf{x}) + \mathcal{O}(\varepsilon^2)$ .

Then we proceed to first order, using the expansions of (Equation 2.9) and (Equation 2.10).

It follows that

$$P_1 \mathbf{U}_0 + P_0 \mathbf{U}_1 = \mathbf{u}_1(\mathbf{x}, 0) + \mathcal{O}(\varepsilon^2) = \eta_1(\mathbf{x}) + \mathcal{O}(\varepsilon^2)$$

$$(G_1 - H_1) \mathbf{U}_0 + (G_0 - H_0) \mathbf{U}_1 = \psi_1 - (H_0 \xi_1 + H_1 \xi_0) + \mathcal{O}(\varepsilon^2).$$

Note that all the first order operators and values depend on the shape of the interface  $\mathbf{g}(\mathbf{x}) = \varepsilon f(\mathbf{x})$ , so that we can write  $P_1, \mathbf{U}_1, G_1, H_1, \psi_1, \xi_1$  as  $P_1(\mathbf{g}), \mathbf{U}_1(\mathbf{g}), G_1(\mathbf{g}), H_1(\mathbf{g}), \psi_1(\mathbf{g}), \xi_1(\mathbf{g})$ .

Writing it in matrix form, we can see the equations more clearly,

$$\begin{pmatrix} P_0 & P_1(\cdot) \mathbf{U}_0 \\ G_0 - H_0 & Q(\cdot) \end{pmatrix} \begin{pmatrix} \mathbf{U}_1 \\ \mathbf{g} \end{pmatrix} = \begin{pmatrix} \eta_1 \\ 0 \end{pmatrix},$$

where  $Q(\cdot) = (G_1 - H_1)(\cdot) \mathbf{U}_0 - \psi_1(\cdot) + H_0 \xi_1(\cdot) + H_1(\cdot) \xi_0$ , which depends on  $\mathbf{g}(\mathbf{x})$ .

**Remark 2.4.1.** As we mentioned earlier § 2.3.2, the operator  $P_0^{-1}$  is ill-conditioned, which will potentially lead to numerical instability. However the instability is also a very common characteristic of inverse problems (18) and it is not surprising to appear here.

### 2.4.2 Numerical Results for 2D Reconstruction

The numerical parameters of our experiment are listed in the following table,

TABLE VI

PARAMETERS USED FOR INVERSE SOLVER SIMULATIONS		
Parameter	value	meaning
N	1,2,3	perturbation orders for the forward solver
nx	16	number of grid points in x direction
$\alpha$	0.1	angle of incident radiation
$k_u$	1	magnitude of wavenumber in the upper layer
$k_v$	0.5	magnitude of wavenumber in the lower layer
d	$10\pi$	the period of the structure
$\epsilon$	$10^{-1}, 10^{-2}, 10^{-3}, 10^{-4}$	the magnitude of perturbation
$\bar{g}$	-4.0	the average depth of the interface

Note that the parameter N is only used in the forward solver to generate data on the surface.

The the inverse solver is implemented based on linear model that will take the data from the

forward solver and recover the interface shape. We conducted several experiments with the inverse solver, but here we focus on two profiles as the shape of interface: a cosine profile

$$f_1 = \cos(x),$$

which is very smooth and has a very simple representation in the Fourier side. The other is Lipschitz profile which is shown in Figure 10.

Note that the input surface data for our inverse solver is generated by our forward solver. When we set the perturbation order of our forward solver  $N$  to different numbers, we will have different input data (with different orders of accuracy). We first tested our linear inverse solver with  $N = 1, 2, 3$ , and the result is shown in Figures 9 to 11.

**Remark 2.4.2.** From the results, we can see that when we set  $N = 1$  (Figure 11), the error is very small which is close to machine precision. That is because our inverse solver is linear, which is the exact inverse of the forward solver when  $N = 1$ , no doubt it generates such good results. When  $N$  is larger, we can see decreased accuracy for the inverse solver. More interestingly, we notice that the greatest error is contributed by the second order, as we can see little difference between the graph of the case  $N = 2$  (Figure 12) and  $N = 3$  (Figure 13). This gives us confidence to develop an iterative inverse solver which will generalize the linear model to a general  $n$ -th order accurate inverse solver. A similar approach can be found in the work of Malcolm and Nicholls (63).

In addition, to address the criticism of committing an “inverse crime” (18), we conducted experiments on the input data with two types of noise. The first type is relative noise, which is defined as,

$$\eta_1 = \eta(1 + M \cdot (2U(0, 1) - 1))$$

where  $M$ , the magnitude of the noise is set to be 0.001, and the results we get are shown in Figure 14. The second type is absolute noise, which is defined as,

$$\eta_2 = \eta + M \cdot |\eta| (2U(0, 1) - 1)$$

where  $M = 0.001$ , and the results we get are shown in Figure 15.

**Remark 2.4.3.** From both Figure 14 and Figure 15, we can see that noise affects the accuracy of our inverse solver greatly, especially absolute noise. Also, in both cases, the impact of the noise tends to be larger on the smooth cosine profile rather than the non-smooth Lipschitz profile, which is reasonable based on the fact that the Fourier coefficients of the cosine profile are zero with only two exceptions, while the Lipschitz profile has all non-zero Fourier coefficients. To achieve a better result, we are also trying to introduce the Tikhonov Regularization technique(69) into our linear model, which will enhance the performance of the inverse solver if we choose an appropriate regularizing parameter(62).

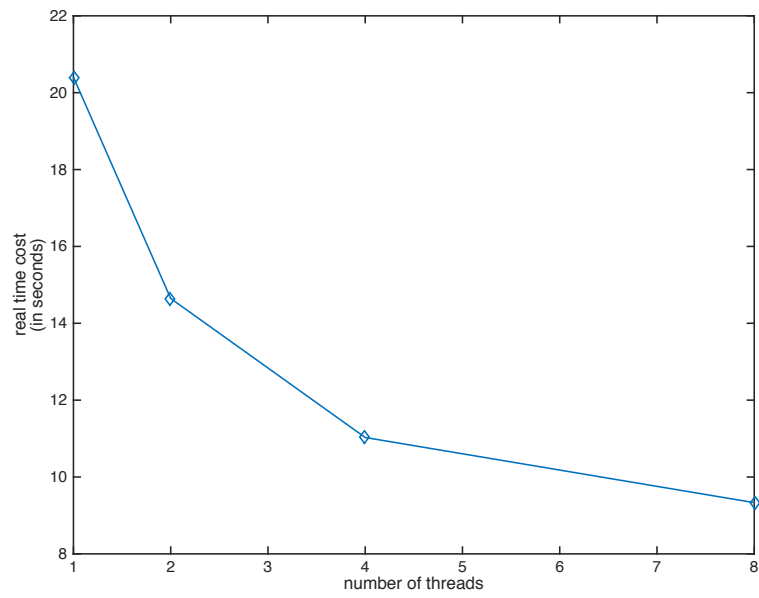


Figure 5. Plot of real time cost versus number of threads for the cosine profile.

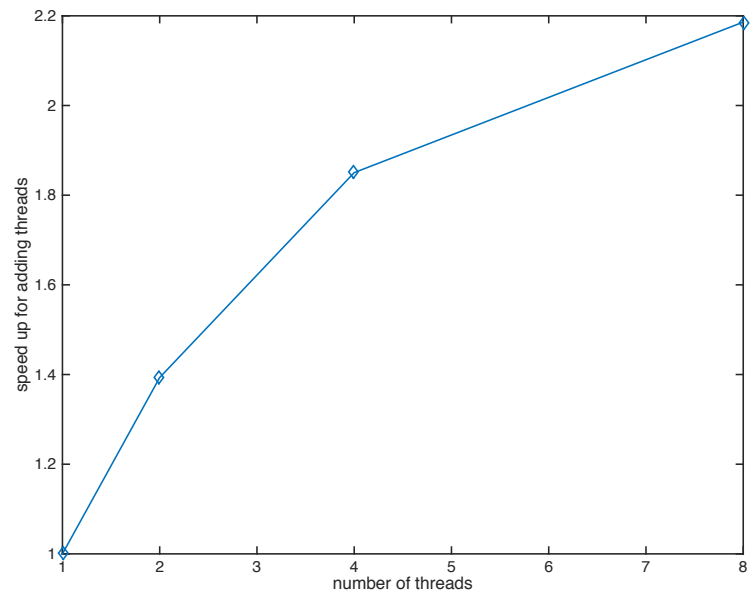


Figure 6. Plot of speedup versus number of threads for the cosine profile.

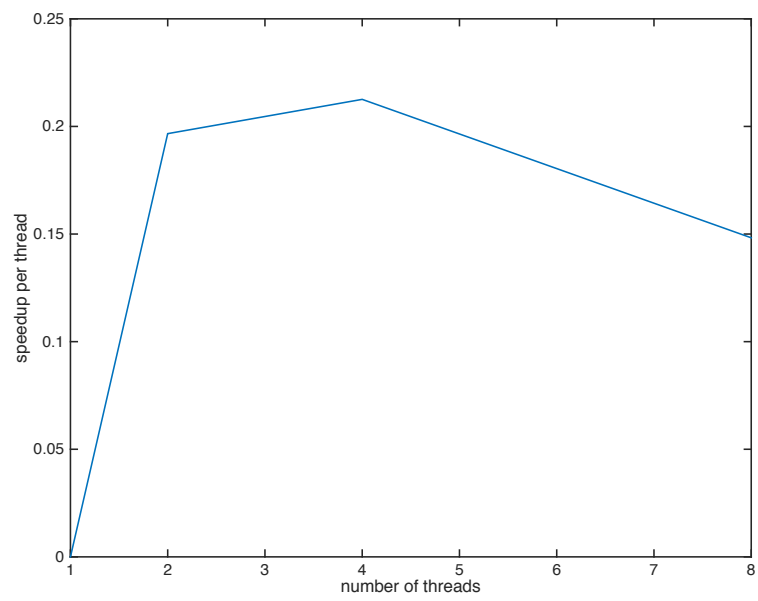


Figure 7. Plot of speedup efficiency per thread versus number of threads for the cosine profile.

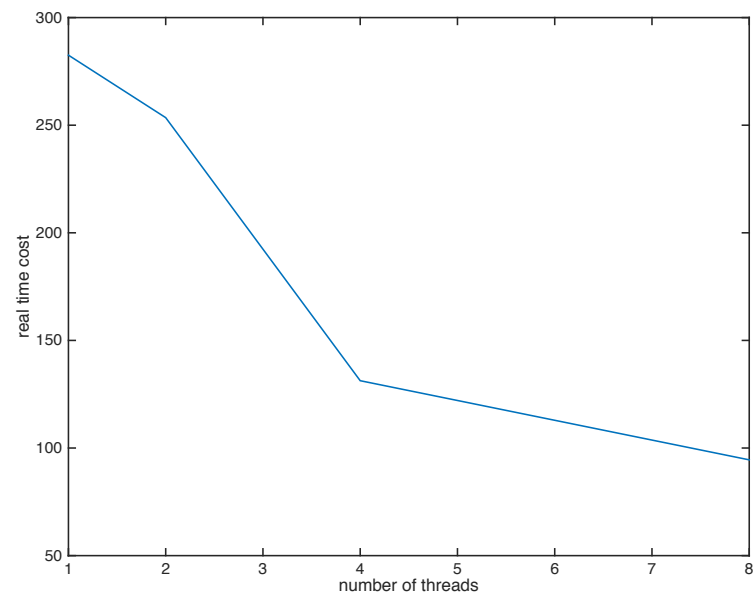


Figure 8. Plot of real time cost versus number of threads for the cosine profile using FFTW MPI.

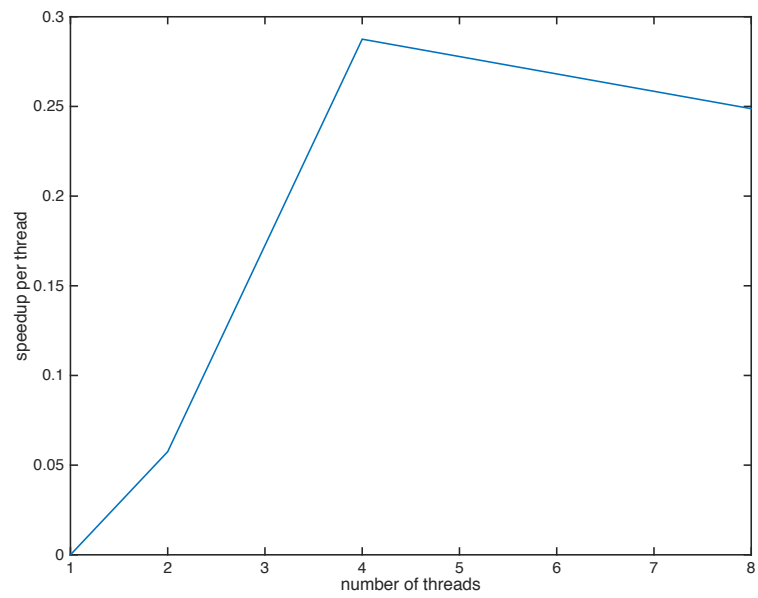


Figure 9. Plot of speedup efficiency per thread versus number of threads for the cosine profile using FFTW MPI.

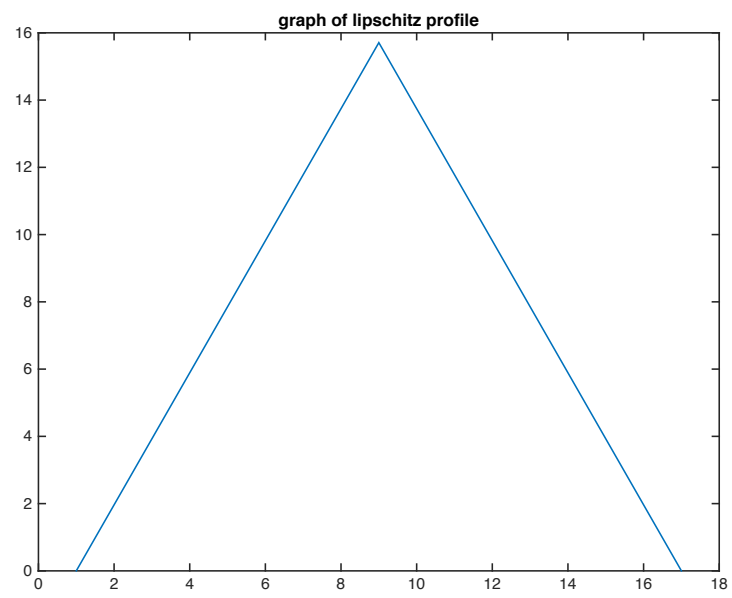


Figure 10. Lipschitz Profile.

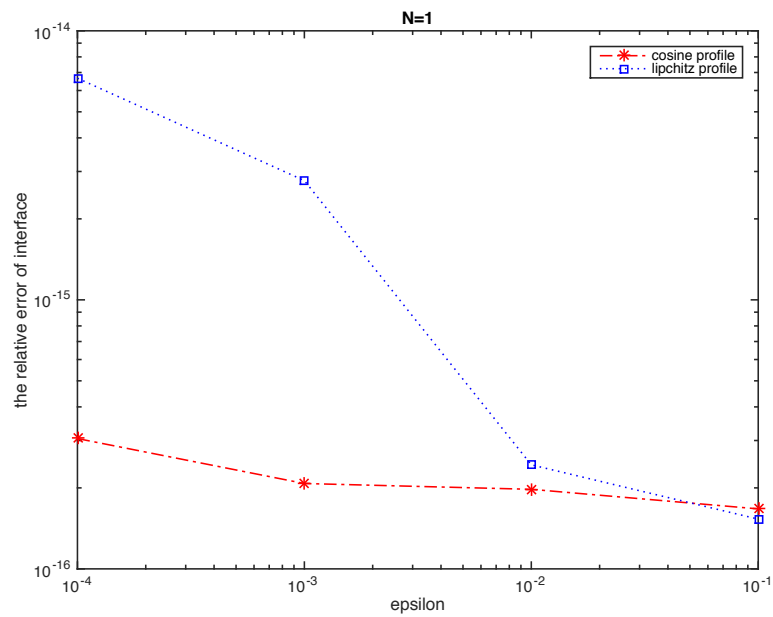


Figure 11. Relative  $L_\infty$  error in reconstructed solution when  $N = 1$ .

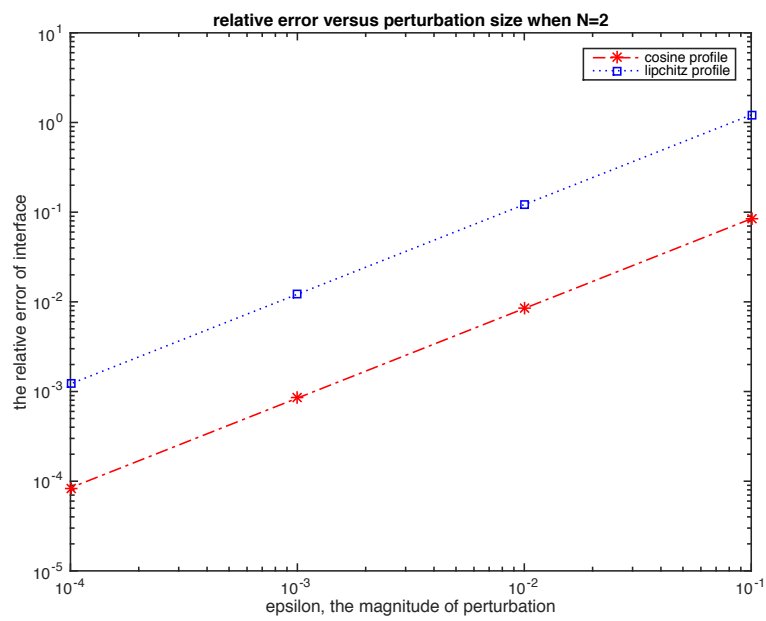


Figure 12. Relative  $L_\infty$  error in reconstructed solution when  $N = 2$ .

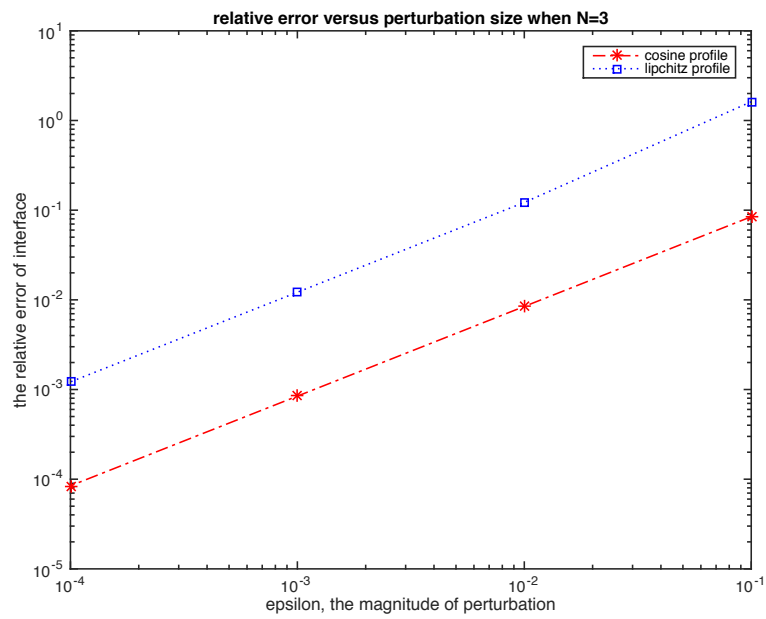


Figure 13. Relative  $L_\infty$  error in reconstructed solution when  $N = 3$ .

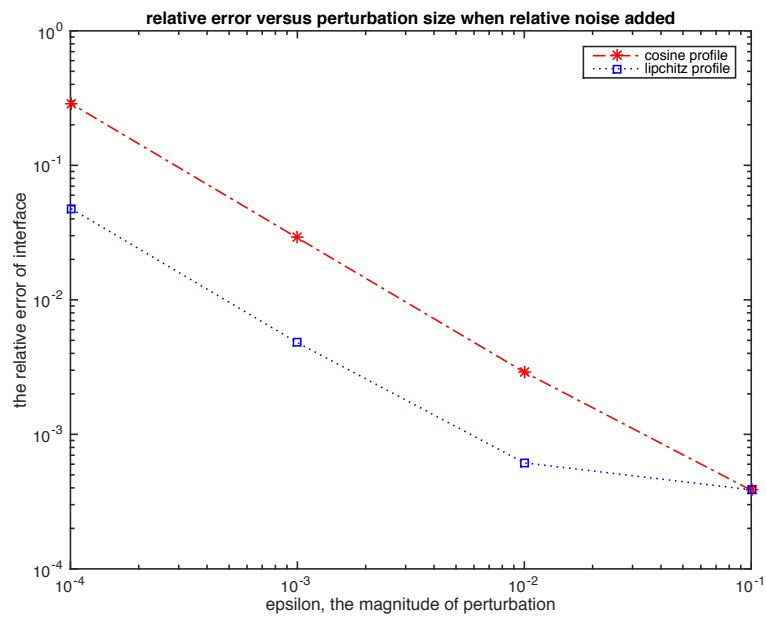


Figure 14. Relative  $L_\infty$  error in reconstructed solution when relative noise is added.

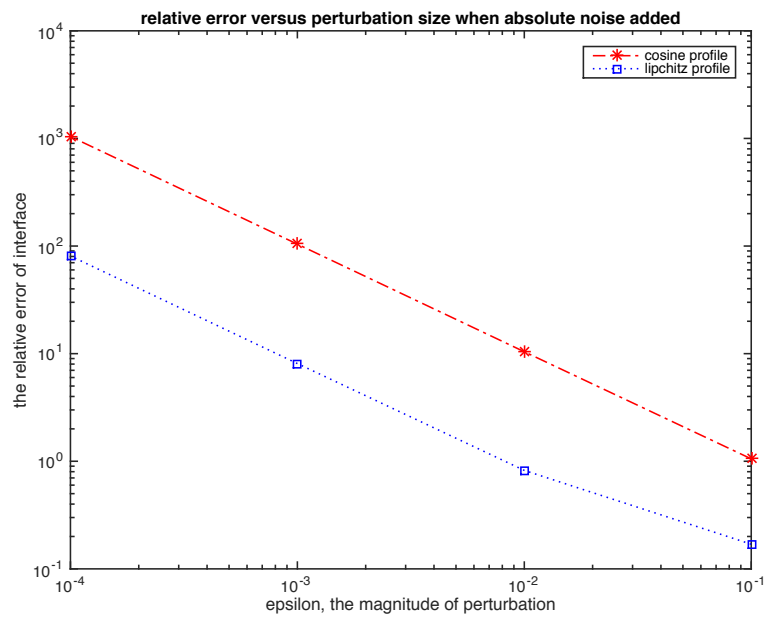


Figure 15. Relative  $L_\infty$  error in reconstructed solution when absolute noise is added.

## CHAPTER 3

### CONCLUSION

The work of this thesis fits into three categories.

First, we generalized the concept of DNO to DTO when the governing equations are Navier's equations. These formulas are far more complicated due to the fact that waves propagating in elastic bodies have P- and S- wave components with different speeds and directions. Although the computational complexity is huge due to the recursive nature of DTO, we lowered the overall complexity of the algorithm by storing the value of the DTO acting on a set of Fourier basis functions in 3 dimensional space.

Secondly, for solutions of the Helmholtz equation, we derived the formulas for the DNO in the 3 dimensional case, which is more complicated than the work done in (63). We designed a robust and rapidly convergent Operator Expansions numerical algorithm to solve DNO, and implemented the solver in a parallel fashion in both 2D and 3D cases, utilizing OpenMp as well as FFTW MPI.

Lastly, we focused our attention on the inverse solver for the Helmholtz equation to recover the shape of a layer interface in 2D layered medium. With the help of the previously built forward solver, we were able to design a linear model for the inverse solver, and the solver showed satisfying accuracy in the case when surface data is from the linear model. To achieve higher order accuracy, we will also try to generalize this linear model to an iterative non-linear model, which should generate good results based on our current experiment. In addition,

we investigated the cases when we have data with two types of noise, and produced some enlightening results. Tikhonov regularization is the next technique we are deciding to try to enhance the performance of the inverse solver when the surface data contains noise.

## APPENDIX

### RECURSIVE FORMULAS FOR THE $\mathbf{U}^{(N)}$ , $\mathbf{K}^{(N)}$ , AND $\mathbf{E}_{ij}^{(N)}$

Of crucial importance to our Operator Expansions approach outlined in § 1.2.2 are forms for the  $\{\mathbf{U}^{(n)}, \mathbf{K}^{(n)}, \mathbf{E}_{ij}^{(n)}\}$ , and in this section we briefly derive these. We begin by recalling the  $\alpha$ -quasiperiodic outgoing solution of the time-harmonic Navier's equation, c.f. (Equation 1.15),

$$\mathbf{u}(\mathbf{x}; \mathbf{p}) = (i\kappa^{(1)}(\mathbf{p}))\hat{\Phi}(\mathbf{p})e^{i\kappa^{(1)}(\mathbf{p})\cdot\mathbf{x}} + \left\{ (i\kappa^{(2)}(\mathbf{p})) \times \hat{\Psi}(\mathbf{p}) \right\} e^{i\kappa^{(2)}(\mathbf{p})\cdot\mathbf{x}},$$

and the surface quantities, c.f. (Equation 1.16),

$$\mathbf{U}(\tilde{\mathbf{x}}; \mathbf{g}, \mathbf{p}) = \mathbf{u}(\tilde{\mathbf{x}}, \mathbf{g}(\tilde{\mathbf{x}}); \mathbf{p})$$

$$\mathbf{K}(\tilde{\mathbf{x}}; \mathbf{g}, \mathbf{p}) = \partial_k \mathbf{u}_k(\tilde{\mathbf{x}}, \mathbf{g}(\tilde{\mathbf{x}}); \mathbf{p})$$

$$\mathbf{E}_{ij}(\tilde{\mathbf{x}}; \mathbf{g}, \mathbf{p}) = \{\partial_j \mathbf{u}_i(\tilde{\mathbf{x}}, \mathbf{g}(\tilde{\mathbf{x}}); \mathbf{p}) + \partial_i \mathbf{u}_j(\tilde{\mathbf{x}}, \mathbf{g}(\tilde{\mathbf{x}}); \mathbf{p})\}.$$

We begin with the  $\mathbf{U}^{(n)}$  by writing

$$\mathbf{U}(\tilde{\mathbf{x}}; \varepsilon \mathbf{f}, \mathbf{p}) = \left\{ (i\kappa^{(1)}(\mathbf{p}))\hat{\Phi}(\mathbf{p})e^{i\gamma^{(1)}(\mathbf{p})\varepsilon \mathbf{f}} + (i\kappa^{(2)}(\mathbf{p})) \times \hat{\Psi}(\mathbf{p})e^{i\gamma^{(2)}(\mathbf{p})\varepsilon \mathbf{f}} \right\} e^{i\alpha(\mathbf{p})\cdot\tilde{\mathbf{x}}}$$

## APPENDIX (Continued)

so that

$$\sum_{n=0}^{\infty} \mathbf{U}^{(n)} \varepsilon^n = \sum_{n=0}^{\infty} \varepsilon^n F_n \left\{ (i\gamma^{(1)}(\mathbf{p}))^n (i\kappa^{(1)}(\mathbf{p})) \hat{\Phi}(\mathbf{p}) + (i\gamma^{(2)}(\mathbf{p}))^n (i\kappa^{(2)}(\mathbf{p})) \times \hat{\Psi}(\mathbf{p}) \right\} e^{i\alpha(\mathbf{p}) \cdot \bar{\mathbf{x}}},$$

where  $F_n = f^n/n!$ . Thus

$$\begin{aligned} \mathbf{U}^{(0)} &= \left\{ (i\kappa^{(1)}(\mathbf{p})) \hat{\Phi}(\mathbf{p}) + (i\kappa^{(2)}(\mathbf{p})) \times \hat{\Psi}(\mathbf{p}) \right\} e^{i\alpha(\mathbf{p}) \cdot \bar{\mathbf{x}}} \\ &= \left\{ (i\kappa^{(1)}(\mathbf{p})) \mathcal{L}_\phi [\hat{\xi}(\mathbf{p})] + (i\kappa^{(2)}(\mathbf{p})) \times \mathcal{L}_\psi [\hat{\xi}(\mathbf{p})] \right\} e^{i\alpha(\mathbf{p}) \cdot \bar{\mathbf{x}}} \\ &= \hat{\xi}(\mathbf{p}) e^{i\alpha(\mathbf{p}) \cdot \bar{\mathbf{x}}}, \end{aligned}$$

and, for  $n > 0$ ,

$$\begin{aligned} \mathbf{U}^{(n)} &= F_n \left\{ (i\gamma^{(1)}(\mathbf{p}))^n (i\kappa^{(1)}(\mathbf{p})) \hat{\Phi}(\mathbf{p}) + (i\gamma^{(2)}(\mathbf{p}))^n (i\kappa^{(2)}(\mathbf{p})) \times \hat{\Psi}(\mathbf{p}) \right\} e^{i\alpha(\mathbf{p}) \cdot \bar{\mathbf{x}}} \\ &= F_n \left\{ (i\gamma^{(1)}(\mathbf{p}))^n (i\kappa^{(1)}(\mathbf{p})) \mathcal{L}_\phi [\hat{\xi}(\mathbf{p})] + (i\gamma^{(2)}(\mathbf{p}))^n (i\kappa^{(2)}(\mathbf{p})) \times \mathcal{L}_\psi [\hat{\xi}(\mathbf{p})] \right\} e^{i\alpha(\mathbf{p}) \cdot \bar{\mathbf{x}}}. \end{aligned}$$

Moving to  $\mathbf{K}^{(n)}$  we write

$$\mathbf{K}(\bar{\mathbf{x}}; \varepsilon f, \mathbf{p}) = - \left| \kappa^{(1)}(\mathbf{p}) \right|^2 \hat{\Phi}(\mathbf{p}) e^{i\gamma^{(1)}(\mathbf{p}) \varepsilon f} e^{i\alpha(\mathbf{p}) \cdot \bar{\mathbf{x}}},$$

so that

$$\sum_{n=0}^{\infty} \mathbf{K}^{(n)} \varepsilon^n = - \sum_{n=0}^{\infty} \varepsilon^n F_n (i\gamma^{(1)}(\mathbf{p}))^n \left| \kappa^{(1)}(\mathbf{p}) \right|^2 \hat{\Phi}(\mathbf{p}) e^{i\alpha(\mathbf{p}) \cdot \bar{\mathbf{x}}}.$$

## APPENDIX (Continued)

Thus

$$\begin{aligned} \mathcal{K}^{(0)} &= - \left| \kappa^{(1)}(\mathbf{p}) \right|^2 \hat{\Phi}(\mathbf{p}) e^{i\alpha(\mathbf{p}) \cdot \tilde{\mathbf{x}}} \\ &= - \left| \kappa^{(1)}(\mathbf{p}) \right|^2 \mathcal{L}_\phi [\hat{\xi}(\mathbf{p})] e^{i\alpha(\mathbf{p}) \cdot \tilde{\mathbf{x}}}, \end{aligned}$$

and, for  $n > 0$ ,

$$\begin{aligned} \mathcal{K}^{(n)} &= -F_n(i\gamma^{(1)}(\mathbf{p}))^n \left| \kappa^{(1)}(\mathbf{p}) \right|^2 \hat{\Phi}(\mathbf{p}) e^{i\alpha(\mathbf{p}) \cdot \tilde{\mathbf{x}}} \\ &= -F_n(i\gamma^{(1)}(\mathbf{p}))^n \left| \kappa^{(1)}(\mathbf{p}) \right|^2 \mathcal{L}_\phi [\hat{\xi}(\mathbf{p})] e^{i\alpha(\mathbf{p}) \cdot \tilde{\mathbf{x}}}. \end{aligned}$$

To close, consider  $E_{ij}^{(n)}$  by writing

$$\begin{aligned} E_{ij}(\tilde{\mathbf{x}}; \varepsilon f, \mathbf{p}) &= \left\{ 2(i\kappa_j^{(1)}(\mathbf{p}))(i\kappa_i^{(1)}(\mathbf{p})) \hat{\Phi}(\mathbf{p}) e^{i\gamma^{(1)}(\mathbf{p}) \varepsilon f} \right. \\ &\quad \left. + \left[ (i\kappa_j^{(2)}(\mathbf{p})) \left\{ (i\kappa^{(2)}(\mathbf{p})) \times \hat{\Psi}(\mathbf{p}) \right\}_i + (i\kappa_i^{(2)}(\mathbf{p})) \left\{ (i\kappa^{(2)}(\mathbf{p})) \times \hat{\Psi}(\mathbf{p}) \right\}_j \right] e^{i\gamma^{(2)}(\mathbf{p}) \varepsilon f} \right\} e^{i\alpha(\mathbf{p}) \cdot \tilde{\mathbf{x}}}, \end{aligned}$$

so that

$$\begin{aligned} \sum_{n=0}^{\infty} E_{ij}^{(n)} \varepsilon^n &= \sum_{n=0}^{\infty} \varepsilon^n F_n \left\{ 2(i\gamma^{(1)}(\mathbf{p}))^n (i\kappa_j^{(1)}(\mathbf{p}))(i\kappa_i^{(1)}(\mathbf{p})) \hat{\Phi}(\mathbf{p}) \right. \\ &\quad \left. + (i\gamma^{(2)}(\mathbf{p}))^n \left[ (i\kappa_j^{(2)}(\mathbf{p})) \left\{ (i\kappa^{(2)}(\mathbf{p})) \times \hat{\Psi}(\mathbf{p}) \right\}_i + (i\kappa_i^{(2)}(\mathbf{p})) \left\{ (i\kappa^{(2)}(\mathbf{p})) \times \hat{\Psi}(\mathbf{p}) \right\}_j \right] \right\} e^{i\alpha(\mathbf{p}) \cdot \tilde{\mathbf{x}}}. \end{aligned}$$

## APPENDIX (Continued)

Thus

$$\begin{aligned}
E_{ij}^{(0)} &= \left\{ 2(i\kappa_j^{(1)}(\mathbf{p}))(i\kappa_i^{(1)}(\mathbf{p}))\hat{\Phi}(\mathbf{p}) \right. \\
&\quad + \left[ (i\kappa_j^{(2)}(\mathbf{p})) \left\{ (i\kappa^{(2)}(\mathbf{p})) \times \hat{\Psi}(\mathbf{p}) \right\}_i \right. \\
&\quad \left. \left. + (i\kappa_i^{(2)}(\mathbf{p})) \left\{ (i\kappa^{(2)}(\mathbf{p})) \times \hat{\Psi}(\mathbf{p}) \right\}_j \right] \right\} e^{i\alpha(\mathbf{p}) \cdot \bar{\mathbf{x}}} \\
&= - \left\{ 2(\kappa_j^{(1)}(\mathbf{p}))(\kappa_i^{(1)}(\mathbf{p}))\mathcal{L}_\Phi [\hat{\Xi}(\mathbf{p})] \right. \\
&\quad + \left[ (\kappa_j^{(2)}(\mathbf{p})) \left\{ (\kappa^{(2)}(\mathbf{p})) \times \mathcal{L}_\Psi [\hat{\Xi}(\mathbf{p})] \right\}_i \right. \\
&\quad \left. \left. + (\kappa_i^{(2)}(\mathbf{p})) \left\{ (\kappa^{(2)}(\mathbf{p})) \times \mathcal{L}_\Psi [\hat{\Xi}(\mathbf{p})] \right\}_j \right] \right\} e^{i\alpha(\mathbf{p}) \cdot \bar{\mathbf{x}}},
\end{aligned}$$

and, for  $n > 0$ ,

$$\begin{aligned}
E_{ij}^{(n)} &= F_n \left\{ 2(i\gamma^{(1)}(\mathbf{p}))^n (i\kappa_j^{(1)}(\mathbf{p}))(i\kappa_i^{(1)}(\mathbf{p}))\hat{\Phi}(\mathbf{p}) \right. \\
&\quad + (i\gamma^{(2)}(\mathbf{p}))^n \left[ (i\kappa_j^{(2)}(\mathbf{p})) \left\{ (i\kappa^{(2)}(\mathbf{p})) \times \hat{\Psi}(\mathbf{p}) \right\}_i \right. \\
&\quad \left. \left. + (i\kappa_i^{(2)}(\mathbf{p})) \left\{ (i\kappa^{(2)}(\mathbf{p})) \times \hat{\Psi}(\mathbf{p}) \right\}_j \right] \right\} e^{i\alpha(\mathbf{p}) \cdot \bar{\mathbf{x}}} \\
&= -F_n \left\{ 2(i\gamma^{(1)}(\mathbf{p}))^n (\kappa_j^{(1)}(\mathbf{p}))(\kappa_i^{(1)}(\mathbf{p}))\mathcal{L}_\Phi [\hat{\Xi}(\mathbf{p})] \right. \\
&\quad + (i\gamma^{(2)}(\mathbf{p}))^n \left[ (\kappa_j^{(2)}(\mathbf{p})) \left\{ (\kappa^{(2)}(\mathbf{p})) \times \mathcal{L}_\Psi [\hat{\Xi}(\mathbf{p})] \right\}_i \right. \\
&\quad \left. \left. + (\kappa_i^{(2)}(\mathbf{p})) \left\{ (\kappa^{(2)}(\mathbf{p})) \times \mathcal{L}_\Psi [\hat{\Xi}(\mathbf{p})] \right\}_j \right] \right\} e^{i\alpha(\mathbf{p}) \cdot \bar{\mathbf{x}}}.
\end{aligned}$$

## APPENDIX

### AUTHOR AND USER RIGHTS OF JOURNAL OF COMPUTATIONAL PHYSICS

As a journal author, you have rights for a large range of uses of your article, including use by your employing institute or company(including usage in a thesis or dissertation ). These rights can be exercised without the need to obtain specific permission.

## CITED LITERATURE

1. Fang, Z. and Nicholls, D. P.: An operator expansions method for computing Dirichlet–Neumann operators in linear elasticity. Journal of Computational Physics, 2014.
2. Billingham, J. and King, A. C.: Wave motion. Cambridge Texts in Applied Mathematics. Cambridge, Cambridge University Press, 2000.
3. ed. C. Godrèche Solids far from equilibrium. Cambridge, Cambridge University Press, 1992.
4. Virieux, J. and Operto, S.: An overview of full-waveform inversion in exploration geophysics. Geophysics, 74(6):WCC1–WCC26, 2009.
5. Bleibinhaus, F. and Rondenay, S.: Effects of surface scattering in full-waveform inversion. Geophysics, 74(6):WCC69–WCC77, 2009.
6. Achenbach, J. D.: Wave Propagation in Elastic Solids. Amsterdam, North–Holland, 1973.
7. Moczo, P., Robertsson, J., and Eisner, L.: The finite-difference time-domain method for modeling of seismic wave propagation. Advances in Geophysics, 48:421, 2007.
8. Pratt, R. G.: Frequency-domain elastic wave modeling by finite differences: A tool for crosshole seismic imaging. Geophysics, 55(5):626–632, 1990.
9. Zienkiewicz, O. C.: The Finite Element Method in Engineering Science, 3rd ed.. New York, McGraw-Hill, 1977.
10. Koketsu, K., Fujiwara, H., and Ikegami, Y.: Finite-element simulation of seismic ground motion with a voxel mesh. Journal Pure and Applied Geophysics, 161(11-12), 2004.
11. Komatitsch, D. and Tromp, J.: Spectral-element simulations of global seismic wave propagation-I. Validation. Geophysical Journal International, 149(2):390–412, 2002.

12. Komatitsch, D. and Tromp, J.: Spectral-element simulations of global seismic wave propagation-II. 3-D models, oceans, rotation, and self-gravitation. Geophysical Journal International, 150(1):303–318, 2002.
13. Sanchez-Sesma, F. and Perez-Rocha, E.: Diffraction of elastic waves by three-dimensional surface irregularities. part II. Bulletin of the Seismological Society of America, 79(1):101, 1989.
14. Bouchon, M.: A review of the discrete wavenumber method. Pure appl. geophys., 160(3):445–465, 2003.
15. Ihlenburg, F.: Finite element analysis of acoustic scattering. New York, Springer-Verlag, 1998.
16. Keller, J. B. and Givoli, D.: Exact nonreflecting boundary conditions. J. Comput. Phys., 82(1):172–192, 1989.
17. Givoli, D.: Recent advances in the DtN FE method. Arch. Comput. Methods Engrg., 6(2):71–116, 1999.
18. Colton, D. and Kress, R.: Inverse acoustic and electromagnetic scattering theory. Berlin, Springer-Verlag, second edition, 1998.
19. Rayleigh, L.: On the dynamical theory of gratings. Proc. Roy. Soc. London, A79:399–416, 1907.
20. Rice, S. O.: Reflection of electromagnetic waves from slightly rough surfaces. Comm. Pure Appl. Math., 4:351–378, 1951.
21. Wait, J. R.: Perturbation analysis for reflection from two-dimensional periodic sea waves. Radio Sci., 6:387–391, 1971.
22. Nayfeh, A. H. and Asfar, O. R.: Parallel-plate waveguide with sinusoidally perturbed boundaries. J. Appl. Phys., 45:4797–4800, 1974.
23. Harper, E. Y. and Labianca, F. M.: Perturbation theory for scattering of sound from a point source by a moving rough surface in the presence of refraction. J. Acoust. Soc. Am., 57:1044–1051, 1975.

24. Harper, E. Y. and Labianca, F. M.: Scattering of sound from a point source by a rough surface progressing over an isovelocity ocean. J. Acoust. Soc. Am., 58:349–364, 1975.
25. Lopez, C., Yndurain, F. J., and Garcia, N.: Iterative series for calculating the scattering of waves from hard corrugated surfaces. Phys. Rev. B, 18:970–972, 1978.
26. Greffet, J. J.: Scattering of electromagnetic waves by rough dielectric surfaces. Phys. Rev. B, 37:6436–6441, 1988.
27. Jackson, D. R., Winebrenner, D. P., and Ishimaru, A.: Comparison of perturbation theories for rough–surface scattering. J. Acoust. Soc. Am., 83:961–969, 1988.
28. Greffet, J. J. and Maassarani, Z.: Scattering of electromagnetic waves by a grating: a numerical evaluation of the iterative–series solution. J. Opt. Soc. Am. A, 7:1483–1493, 1990.
29. Roginsky, J.: Derivation of closed–form expressions for the T matrices of Rayleigh–Rice and extinction–theorem perturbation theories. J. Acoust. Soc. Am., 90:1130–1137, 1991.
30. Milder, D. M.: An improved formalism for rough-surface scattering of acoustic and electromagnetic waves. In Proceedings of SPIE - The International Society for Optical Engineering (San Diego, 1991), volume 1558, pages 213–221. Bellingham, WA, Int. Soc. for Optical Engineering, 1991.
31. Greffet, J. J., Baylard, C., and Versaevel, P.: Diffraction of electromagnetic waves by crossed gratings: a series solution. Opt. Lett., 17:1740–1742, 1992.
32. Kazandjian, L.: Comparison of the Rayleigh-Fourier and extinction theorem methods applied to scattering and transmission at a rough solid-solid interface. J. Acoust. Soc. Am., 92:1679–1691, 1992.
33. Chesneaux, J. M. and A. Wirgin, A.: Response to comments on “reflection from a corrugated surface revisited”. J. Acoust. Soc. Am., 98:1815–1816, 1995.
34. Voronovich, A. G.: Wave scattering from rough surfaces. Berlin, Springer-Verlag, second edition, 1999.

35. Coifman, R., Goldberg, M., Hrycak, T., Israeli, M., and Rokhlin, V.: An improved operator expansion algorithm for direct and inverse scattering computations. Waves Random Media, 9(3):441–457, 1999.
36. Gilbert, F. and Knopoff, L.: Seismic scattering from topographic irregularities. Journal of Geophysical Research, 65(10):3437–3444, 1960.
37. Herrera, I.: A perturbation method for elastic wave propagation: 1. nonparallel boundaries. Journal of Geophysical Research, 69(18):3845–3851, 1964.
38. Woodhouse, J. and Dahlen, F.: The effect of a general aspherical perturbation on the free oscillations of the earth. Geophysical Journal of the Royal Astronomical Society, 53(2):335–354, 1978.
39. Snieder, R.: The influence of topography on the propagation and scattering of surface waves. Physics of the earth and planetary interiors, 44(3):226–241, 1986.
40. Wu, R.-S.: The perturbation method in elastic wave scattering. In Scattering and Attenuation of Seismic Waves, Part II, pages 605–637. Springer, 1989.
41. Nicholls, D. P.: Efficient enforcement of far-field boundary conditions in the transformed field expansions method. Journal of Computational Physics, 230(22):8290–8303, 2011.
42. Milder, D. M.: An improved formalism for wave scattering from rough surfaces. J. Acoust. Soc. Am., 89(2):529–541, 1991.
43. Milder, D. M. and Sharp, H. T.: Efficient computation of rough surface scattering. In Mathematical and numerical aspects of wave propagation phenomena (Strasbourg, 1991), pages 314–322. Philadelphia, PA, SIAM, 1991.
44. Milder, D. M. and Sharp, H. T.: An improved formalism for rough surface scattering. ii: Numerical trials in three dimensions. J. Acoust. Soc. Am., 91(5):2620–2626, 1992.
45. Milder, D. M.: Role of the admittance operator in rough-surface scattering. J. Acoust. Soc. Am., 100(2):759–768, 1996.
46. Milder, D. M.: An improved formalism for electromagnetic scattering from a perfectly conducting rough surface. Radio Science, 31(6):1369–1376, 1996.

47. Bruno, O. P. and Reitich, F.: Numerical solution of diffraction problems: A method of variation of boundaries. J. Opt. Soc. Am. A, 10(6):1168–1175, 1993.
48. Bruno, O. P. and Reitich, F.: Numerical solution of diffraction problems: A method of variation of boundaries. II. Finitely conducting gratings, Padé approximants, and singularities. J. Opt. Soc. Am. A, 10(11):2307–2316, 1993.
49. Bruno, O. P. and Reitich, F.: Numerical solution of diffraction problems: A method of variation of boundaries. III. Doubly periodic gratings. J. Opt. Soc. Am. A, 10(12):2551–2562, 1993.
50. Bruno, O. P. and Reitich, F.: Calculation of electromagnetic scattering via boundary variations and analytic continuation. Appl. Comput. Electromagn. Soc. J., 11(1):17–31, 1996.
51. Bruno, O. P. and Reitich, F.: Boundary–variation solutions for bounded–obstacle scattering problems in three dimensions. J. Acoust. Soc. Am., 104(5):2579–2583, 1998.
52. Nicholls, D. P. and Reitich, F.: A new approach to analyticity of Dirichlet-Neumann operators. Proc. Roy. Soc. Edinburgh Sect. A, 131(6):1411–1433, 2001.
53. Nicholls, D. P. and Reitich, F.: Stability of high-order perturbative methods for the computation of Dirichlet-Neumann operators. J. Comput. Phys., 170(1):276–298, 2001.
54. Nicholls, D. P. and Reitich, F.: Analytic continuation of Dirichlet-Neumann operators. Numer. Math., 94(1):107–146, 2003.
55. Nicholls, D. P. and Reitich, F.: Shape deformations in rough surface scattering: Cancellations, conditioning, and convergence. J. Opt. Soc. Am. A, 21(4):590–605, 2004.
56. Nicholls, D. P. and Reitich, F.: Shape deformations in rough surface scattering: Improved algorithms. J. Opt. Soc. Am. A, 21(4):606–621, 2004.
57. Coifman, R. and Meyer, Y.: Nonlinear harmonic analysis and analytic dependence. In Pseudodifferential operators and applications (Notre Dame, Ind., 1984), pages 71–78. Amer. Math. Soc., 1985.
58. Hu, B. and Nicholls, D. P.: Analyticity of Dirichlet–Neumann operators on Hölder and Lipschitz domains. SIAM J. Math. Anal., 37(1):302–320, 2005.

59. Craig, W. and Sulem, C.: Numerical simulation of gravity waves. Journal of Computational Physics, 108:73–83, 1993.
60. Nicholls, D. P.: Traveling water waves: Spectral continuation methods with parallel implementation. J. Comput. Phys., 143(1):224–240, 1998.
61. Gottlieb, D. and Orszag, S. A.: Numerical analysis of spectral methods: theory and applications. Philadelphia, Pa., Society for Industrial and Applied Mathematics, 1977. CBMS-NSF Regional Conference Series in Applied Mathematics, No. 26.
62. Malcolm, A. and Nicholls, D. P.: Operator expansions and constrained quadratic optimization for interface reconstruction: Impenetrable acoustic media. Wave Motion, 51:23–40, 2014.
63. Malcolm, A. and Nicholls, D. P.: A boundary perturbation method for recovering interface shapes in layered media. Inverse Problems, 27(9):095009, 2011.
64. Frigo, M. and Johnson, S. G.: FFTW: An adaptive software architecture for the FFT. In Proc. 1998 IEEE Intl. Conf. Acoustics Speech and Signal Processing, volume 3, pages 1381–1384. IEEE, 1998.
65. OpenMP Architecture Review Board: OpenMP Application Program Interface, version 4.0 edition, July 2013.
66. Nicholls, D. P. and Taber, M.: Joint analyticity and analytic continuation for Dirichlet–Neumann operators on doubly perturbed domains. J. Math. Fluid Mech., 10(2):238–271, 2008.
67. Nicholls, D. P. and Taber, M.: Detection of ocean bathymetry from surface wave measurements. Euro. J. Mech. B/Fluids, 28(2):224–233, 2009.
68. ed. R. Petit Electromagnetic theory of gratings. Berlin, Springer-Verlag, 1980.
69. Kress, R.: Linear integral equations. New York, Springer-Verlag, second edition, 1999.

VITA

# Zheng Fang

---

## Education

**Phd in Applied Math**, *University of Illinois at Chicago*, Expected June 2015.

GPA: 4.0/4.0

Homepage:<http://www.math.uic.edu/~zfang3/>

**Master in Applied Mathematics**, *University of Illinois at Chicago*, 2012.

GPA: 4.0/4.0

Master exam marks: 157/160

**Master in Computer Science**, *University of Illinois at Chicago*, Expected June 2015.

GPA: 4.0/4.0

**Bachelor of Mathematics**, *University of Science and Technology of China*, June 2010.

GPA: 3.6/4.3

---

## Related Coursework

**Advanced Partial Differential Equations, Numerical Analysis of PDE, Linear & Nonlinear Waves, Asymptotic Methods, Singular Perturbations, Topics in Fluid Mechanics, Computer Algorithms, Object-Oriented Languages & Environments, Supercomputing.**

---

## Work Experience

Summer 2014 **Tech Intern II, Yahoo Mail!, Sunnyvale, CA.**

Summer 2012–Present **Research Assistant**, *University of Illinois at Chicago*.  
Advisor: Professor David Nicholls.

2010–2012 **Teaching Assistant**, *University of Illinois at Chicago*.

---

## Computer Skills

Scientific MATLAB, MATHEMATICA, R  
Development Java, C++, Smalltalk, Python  
Typesetting Latex, Beamer  
Other SQL, CSS, HTML, Linux,